nature cell biology

Tissue elongation requires oscillating contractions of a basal actomyosin network

Li He[1,3], Xiaobo Wang[1,3], Ho Lam Tang[1] and Denise J. Montell[1,2]

Understanding how molecular dynamics leads to cellular behaviours that ultimately sculpt organs and tissues is a major challenge not only in basic developmental biology but also in tissue engineering and regenerative medicine. Here we use live imaging to show that the basal surfaces of *Drosophila* follicle cells undergo a series of directional, oscillating contractions driven by periodic myosin accumulation on a polarized actin network. Inhibition of the actomyosin contractions or their coupling to extracellular matrix (ECM) blocked elongation of the whole tissue, whereas enhancement of the contractions exaggerated it. Myosin accumulated in a periodic manner before each contraction and was regulated by the small GTPase Rho, its downstream kinase, ROCK, and cytosolic calcium. Disrupting the link between the actin cytoskeleton and the ECM decreased the amplitude and period of the contractions, whereas enhancing cell–ECM adhesion increased them. In contrast, disrupting cell–cell adhesions resulted in loss of the actin network. Our findings reveal a mechanism controlling organ shape and an experimental model for the study of the effects of oscillatory actomyosin activity within a coherent cell sheet.

The goal of tissue engineering is to create artificial organs and tissues *in vitro*, which requires understanding not only how each cell type is specified but also how cells cooperate to generate appropriate organ shapes and tissue architectures. The molecular and mechanical mechanisms governing some multicellular morphogenetic movements are beginning to be elucidated[1,2]. For example, periodic contraction of apical networks of actomyosin in *Drosophila* embryos drives apical constriction, which contributes to many morphogenetic movements including mesoderm invagination and dorsal closure. In addition, apical accumulation of myosin specifically at dorsal–ventral (D–V) cell–cell boundaries drives directional cell intercalation during germ band elongation[3–5]. A remaining challenge is to explain the great diversity of morphogenetic processes that occur, and in particular those that do not involve apical constriction. Oogenesis in *Drosophila* serves as a good model system in which to study a variety of cell behaviours during morphogenesis[6,7].

The *Drosophila* ovary is made up of developing egg chambers, each of which produces a single egg. Each egg chamber is composed of 16 germline cells (15 nurse cells and 1 oocyte) surrounded by a monolayer of epithelial follicle cells (Supplementary Information, Fig. S1a). From developmental stage 8 to late stage 10, the egg chamber grows markedly, increases in volume about eightfold, and elongates about 1.7-fold. The cellular and molecular mechanisms regulating the elongation of this tissue are incompletely understood, and contradictory models have been proposed. Apical constriction has been suggested to have a role[8]; however, a quantitative analysis of follicle cell structure found no evidence that apical constriction occurs[9]. The latter study suggested that the increase in egg chamber volume combined with a 'corset' for constraining the increase in volume to the ends of the tissue could account for egg chamber elongation. Follicle cells acquire a polarized array of F-actin near the basal surface, which aligns with extracellular matrix fibres, possibly contributing to the corset, because disruption of cell–matrix adhesion can cause eggs to be rounder[10–13]. However, all previous studies of this process have relied on the analysis of fixed tissue, and thus no dynamic information has been available to assist in elucidating the mechanism.

RESULTS

Oscillation in basal cell surface area correlated with myosin accumulation in *Drosophila* follicle cells

To understand this tissue elongation process better, we used egg-chamber culturing techniques and live imaging[14,15] of E-cadherin fused to green fluorescent protein (cadherin–GFP)[16] to observe dynamic changes in the egg chamber between stages 8 and 10 (Fig. 1a–k; Supplementary Information, Fig. S1b–j; Supplementary Information, Movie 1). During time-lapse imaging, basal cell surfaces showed periodic contraction and relaxation (Fig. 1l, m; Supplementary Information, Movie 2). In contrast, apical surfaces showed smaller, random changes (Supplementary Information, Movie 3).

The basal oscillations bore some resemblance to recently observed pulsation during apical constriction in *Drosophila* embryos[3,4,17–20], which is caused by a periodic accumulation and contraction of apical actomyosin.

[1]Department of Biological Chemistry, Center for Cell Dynamics, Johns Hopkins School of Medicine, 855 North Wolfe Street, Baltimore, Maryland 21205, USA.
[2]Correspondence should be addressed to D.J.M. (e-mail: dmontell@jhmi.edu)
[3]These authors contributed equally to this work.

Received 15 July 2010; accepted 28 October 2010; published online 21 November 2010; DOI:10.1038/ncb2124

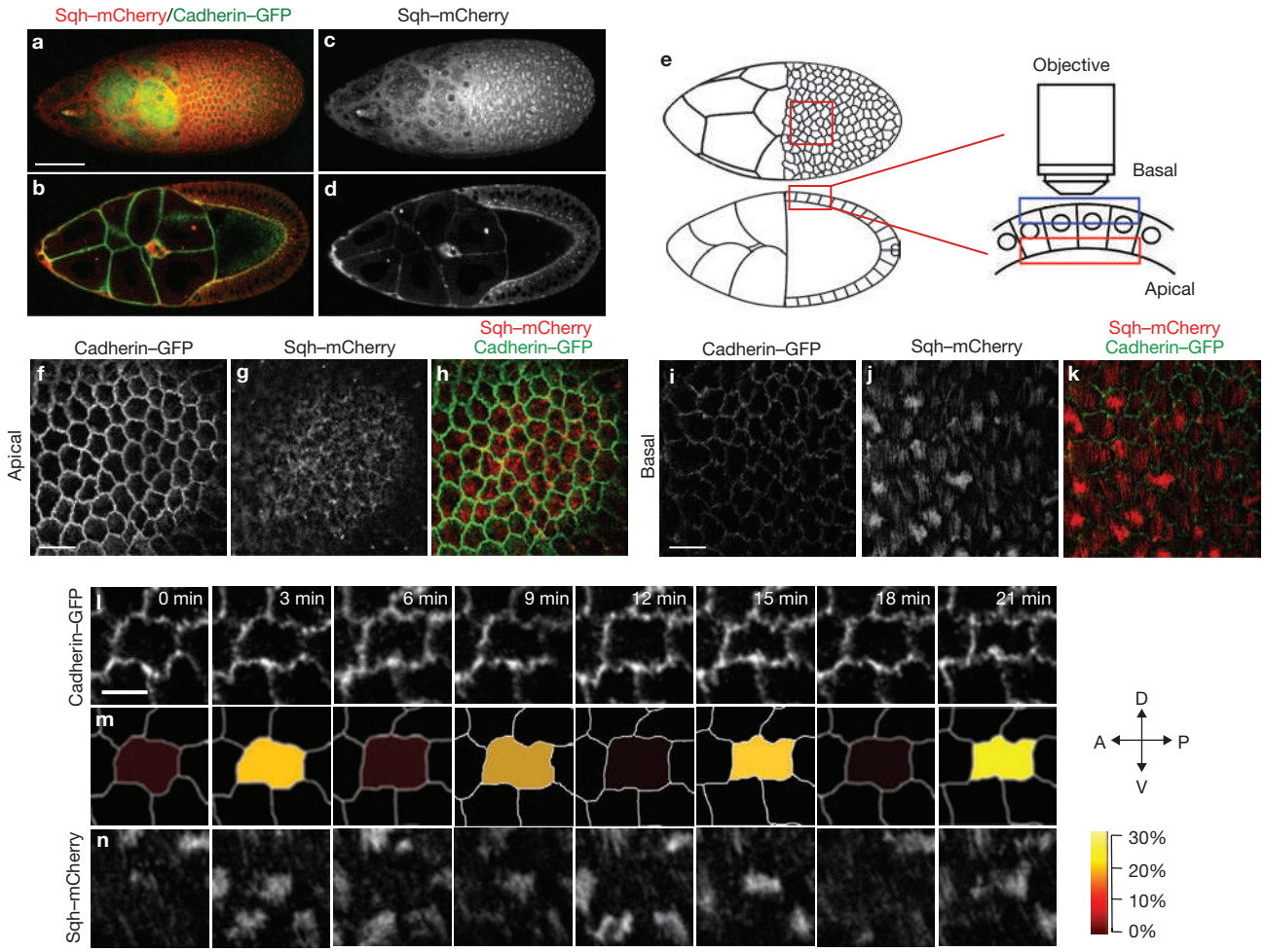

Figure 1 Stage-9 follicle cells undergo rapid periodic contractions and myosin accumulation. (**a**) Surface view of a live, late-stage-9 egg chamber expressing Sqh–mCherry (red) and cadherin–GFP (green). (**b**) Sagittal plane through the centre of the egg chamber. (**c**, **d**). Sqh–mCherry label alone, in the same preparations as in **a** and **b**. Scale bar, 50 μm. (**e**) Schematic drawings of egg chambers in **a** and **b**, and the imaging of the apical and basal regions of the follicle cells. The red boxes in the left panel indicate a typical field of cells. The blue and red boxes on the right indicate the basal and apical focal planes, respectively. (**f**–**k**) Images of late-stage-9 egg chamber expressing Sqh–mCherry (red) and cadherin–GFP (green) at apical and basal focal planes. Scale bar, 20 μm. (**l**–**n**) Time-lapse series of one representative oscillating cell labelled with cadherin–GFP (**i**) and Sqh–mCherry (**n**). The digitized cell contour is colour-coded on the basis of the percentage decrease in surface area relative to the maximum area captured during imaging, as indicated in the heat map (**m**). Scale bar, 10 μm. The A–P and D–V orientations are shown at the right.

We therefore monitored myosin accumulation by using the red fluorescent protein mCherry fused to the myosin regulatory light chain named Spaghetti Squash (Sqh–mCherry)[3]. From still images, apical myosin resembled a random mesh (Fig. 1g, h), whereas basal myosin accumulated in parallel fibres near the basal follicle cell surface with highly variable intensity (Fig. 1j, k). Time-lapse imaging revealed that the variation in intensity was due to repeated cycles of basal myosin accumulation and disappearance from individual cells (Fig. 1n), which were asynchronous. There seemed to be a correlation between myosin accumulation and the decrease in basal cell surface area within each cell (Fig. 1l–n; Supplementary Information, Movie 2).

Quantification and comparison of basal and apical follicle cell activities

To quantify these effects we developed a MATLAB program to automatically track the change of cell geometry and found that the basal area did indeed show clear periodic changes (Fig. 2a). The basal area change was highly polarized, correlating with a change in the length of cells along the D–V axis, whereas we observed little or no change in cell length along the anterior–posterior (A–P) axis (Fig. 2a). The average period of the basal contractions was 6.3 min, with most contraction–relaxation cycles being completed in 5–7 min (Fig. 2b). In contrast, apical cell surfaces showed small, random fluctuations in cell shape (Fig. 2c; Supplementary Information, Movie 3), which were only half the magnitude of the change in basal surface area (Fig. 2d). The apical area change was also symmetrical, whereas the basal membrane activity was fivefold higher in the D–V direction than in the A–P direction (Fig. 2e).

In time-lapse movies, basal myosin underwent marked and periodic changes in concentration (Fig. 2g, h; Supplementary Information, Movie 2), whereas near the apical surface, myosin showed no periodicity (Fig. 2c, h) and was far less dynamic (Fig. 2f). A lateral view showed that myosin accumulated in and then disappeared from a thin layer about 1 μm beneath the basal plasma membrane, rather than moving into and out of the basal plane of focus (Supplementary Information, Movie 4).

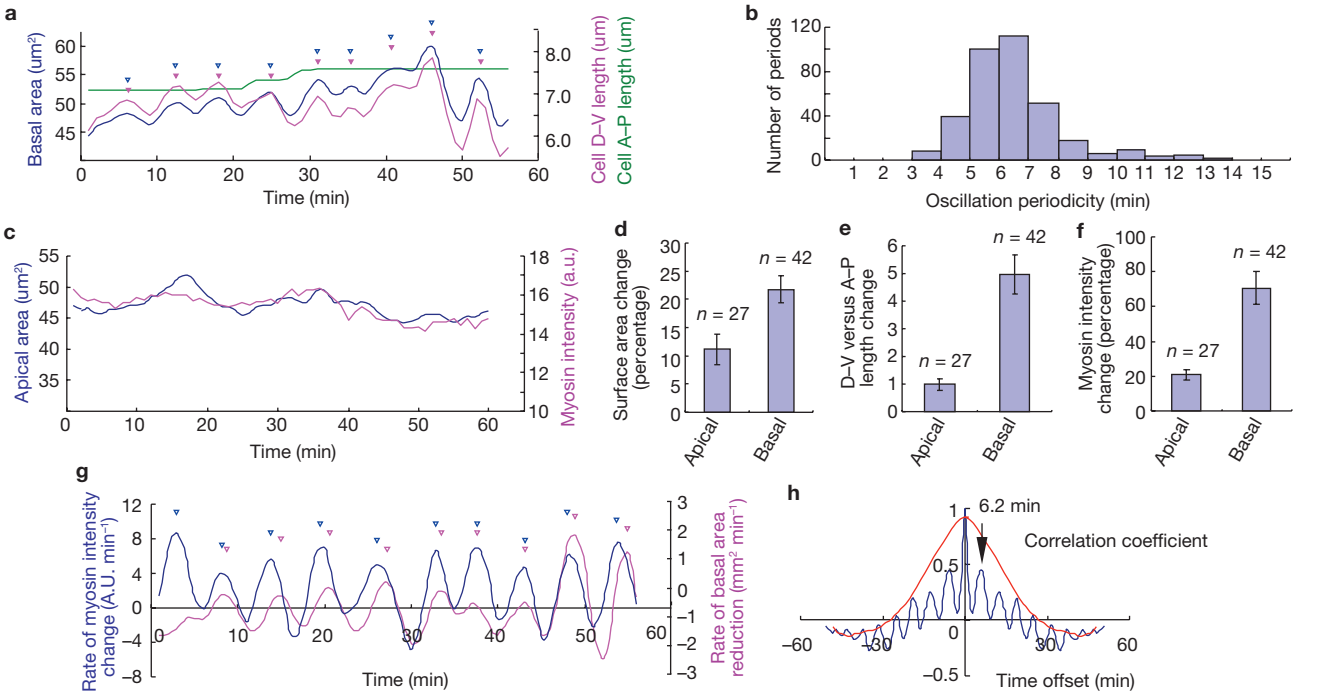

Figure 2 Quantification of basal periodic contraction and comparison with apical activity. (**a**) Dynamic change of basal area, D–V and A–P cell length from one representative cell. Peaks are indicated by arrowheads of the corresponding colour. (**b**) The distribution of periods observed over 375 oscillations with a mean of 6.3 min and s.d. of 1.2 min. (**c**) Change in apical area and apical myosin intensity from one representative cell over time. (**d**) Calculated surface area change for the indicated numbers (*n*) of cells over 30 min of imaging. (**e**) Calculated ratio of D–V to A–P length change over time; *n* is the number of individual cells analysed. (**f**) Changes in apical and basal myosin intensity compared with the average intensity for each, over time; *n* is the number of individual cells analysed. (**g**) Rate of change of myosin intensity (blue) and rate of decrease in basal area (purple) from the same sample. Peaks are marked with arrowheads. (**h**) Autocorrelation of time sequences of apical (red) and basal (blue) myosin intensity. All error bars indicate s.d.

Simultaneous measurement of basal myosin accumulation and cell area showed that the area shrank as myosin accumulated (Fig. 2g; Supplementary Information, Fig. S1k), supporting the notion that the two phenomena might be related. The rate of myosin accumulation correlated well with the rate of contraction of the cell area (Fig. 2g), the former preceding the latter by about 1 min, suggesting that myosin accumulation could in principle cause the decrease in basal surface area.

Basal actin organization

We then used GFP-tagged moesin, an F-actin-binding protein, to reveal dynamic changes in F-actin[21]. As reported previously[10], F-actin forms parallel bundles along basal follicle cell surfaces (Fig. 3a, b). However, in contrast to the periodic, approximately 70% changes in myosin concentration, actin filament density changed by only about 20% over time (Fig. 3c; Supplementary Information, Movie 5). A time correlation analysis showed that, in contrast to the myosin accumulation, the change in F-actin did not precede but rather coincided with the change in myosin intensity (Fig. 3d–g). Together these results suggest that the periodic changes in myosin accumulation were not caused by dynamic changes in F-actin.

Although the periodic myosin accumulation and cell surface area reductions described here resemble the pulsatile contractions that underlie apical constriction during *Drosophila* gastrulation[3,4,18–20], the activity in follicle cells differs in several key respects (Fig. 3j). First, the follicle cell contractions occur near the basal cell surface rather than apically. Second, during apical constriction, myosin fibres accumulate in a randomly oriented meshwork[3], whereas basal myosin fibres in follicle cells were highly organized in parallel bundles along the D–V axis (Fig. 3j; Supplementary Information, Movie 5). Third, the actin filaments change intensity with a similar amplitude to that of myosin in apical constriction[20], whereas there is little change in basal actin in follicle cells (Fig. 3j; Supplementary Information, Movie 5). Fourth, the decrease in apical surface area in the embryo is eventually stabilized by a poorly characterized ratchet mechanism, resulting in a lasting change in cell shape, whereas the change in basal follicle cell shape was temporary (Fig. 3h, i; Supplementary Information, Fig. S2a–j). Last, in the gastrulating embryo the contractions are limited to cells on the ventral side of the embryo, whereas the follicle cell activity occurred all around the egg chamber regardless of cell position along the D–V axis.

Spatial and temporal regulation of periodic myosin accumulation

Although the basal oscillations were not patterned along the D–V axis, we did notice a global spatial and temporal pattern to the myosin accumulation and cellular contractions (Fig. 4a–e; Supplementary Information, Movie 6). The myosin oscillations appeared first in early stage 9 in a band of cells about one-third of the distance from the anterior pole and shifted relatively quickly to the middle part of the egg chamber (Fig. 4a, b). During development, both the average basal myosin intensity and the number of oscillating cells increased until stage 10, by which time almost all follicle cells in contact with the oocyte accumulated basal myosin (Fig. 4b–f), whereas apical myosin changed very little over the same developmental stages (Fig. 4g–k). Nurse-cell-associated follicle cells showed no measurable accumulation of myosin (Fig. 4b–e).

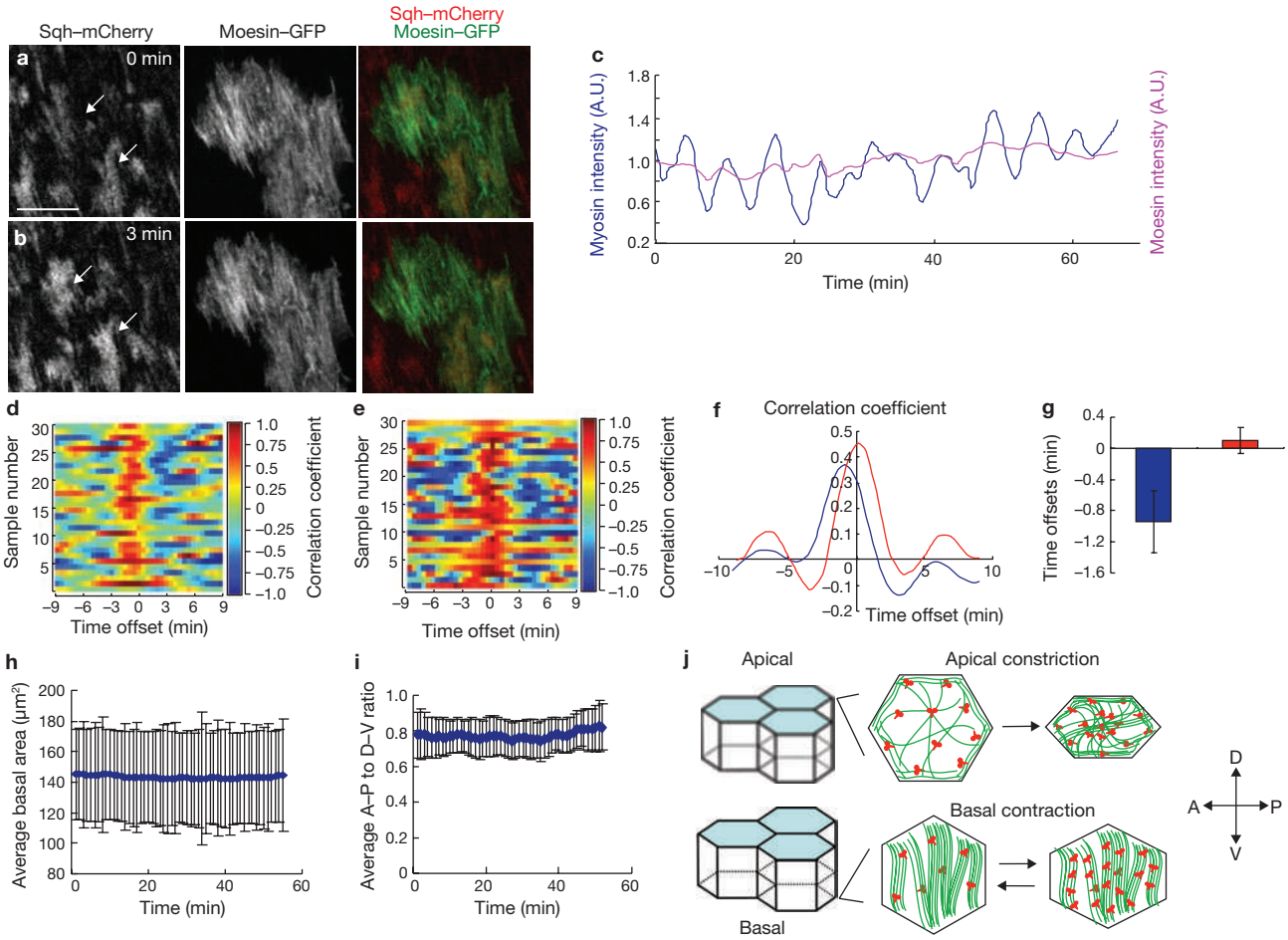

Figure 3 Accumulation of basal myosin on stable actin filaments precedes the basal membrane contraction. (**a**, **b**) Confocal micrographs of a clone of moesin–GFP in cells expressing Sqh–mCherry. Images in **a** and **b** were taken 3 min apart. Myosin intensity changes in two cells (left panel, arrows), whereas moesin-labelled F-actin does not change detectably. Scale bar, 10 μm. (**c**) Quantification of the dynamic change of moesin–GFP and Sqh–mCherry intensity in one oscillating cell. Intensity of each channel was normalized to its mean. (**d**) Correlation between the rate of decrease in basal area and change in myosin intensity. (**e**) Correlation between moesin and myosin intensity. Each row shows the correlation from a different cell as a function of various time offsets. (**f**) Average of all correlation coefficients with different time offsets. The blue line shows the average time-dependent correlation between rate of decrease in area and rate of change in myosin intensity from 43 individual cells. The red line shows the average time-dependent correlation between moesin and myosin intensity from 37 individual cells. The correlation between the rate of basal area reduction and myosin accumulation reaches a maximum at −1 min, suggesting that myosin accumulation precedes area decrease. In contrast, the correlation between myosin intensity and F-actin intensity peaks at 0, indicating that they are virtually simultaneous. (**g**) The position of maximum correlation between contraction rate and intensity change rate (blue) is significantly different from zero with $P < 0.001$, whereas the moesin–myosin correlation (red) is not. Error bars indicate s.d. (**h**) The basal areas of cells ($n = 45$) were calculated and averaged. Even though the basal areas of individual cells fluctuated periodically, the average basal area did not change because the fluctuations were temporary and unsynchronized. (**i**) The ratio of A–P to D–V cell lengths during the time of imaging ($n = 45$). The periodic changes observed in individual cells were neither synchronous nor lasting; therefore no change was detected on average. (**j**) Diagram of different organizations and dynamics of the apical actomyosin for cells undergoing apical constriction versus the basal actomyosin for cells undergoing basal oscillations.

Actomyosin contraction regulates tissue shape

Because the myosin oscillations and overall tissue elongation occur during the same stages of development (Fig. 4a), we speculated that the periodic contractions might contribute to tissue elongation. To test this, we first took a pharmacological approach to interfere with actin and myosin function (Supplementary Information, Movie 7). In comparison with control samples treated with dimethylsulphoxide (DMSO; Fig. 5a, d, h), the addition of cytochalasin D (cytoD), an actin filament destabilizer, greatly decreased the levels of basal actin and myosin filaments and blocked the oscillations (Fig. 5b, e, g, h). This also resulted in a clear relaxation and expansion of egg chamber width (Fig. 5b, g). In contrast, addition of the calcium ionophore ionomycin, which promotes the contraction of actomyosin filaments in smooth-muscle cells[22,23], markedly increased the amount of basal myosin (Fig. 5f, h) and elongated the egg chamber (Fig. 5c, g; Supplementary Information, Movie 7). The microtubule destabilizer colchicine had no effect on the myosin oscillation but did deform the tissue, resulting in irregularly shaped egg chambers (Supplementary Information, Fig. S3j). Apical actin and myosin showed similar changes in response to treatment with CytoD and with ionomycin (Supplementary Information, Fig. 3d–g), so this experiment did not rule out a contribution of the apical cytoskeleton; however, the lack of polarization and dynamics made the apical cytoskeleton a less likely candidate for involvement in this directional tissue elongation. Taken together, these findings indicate

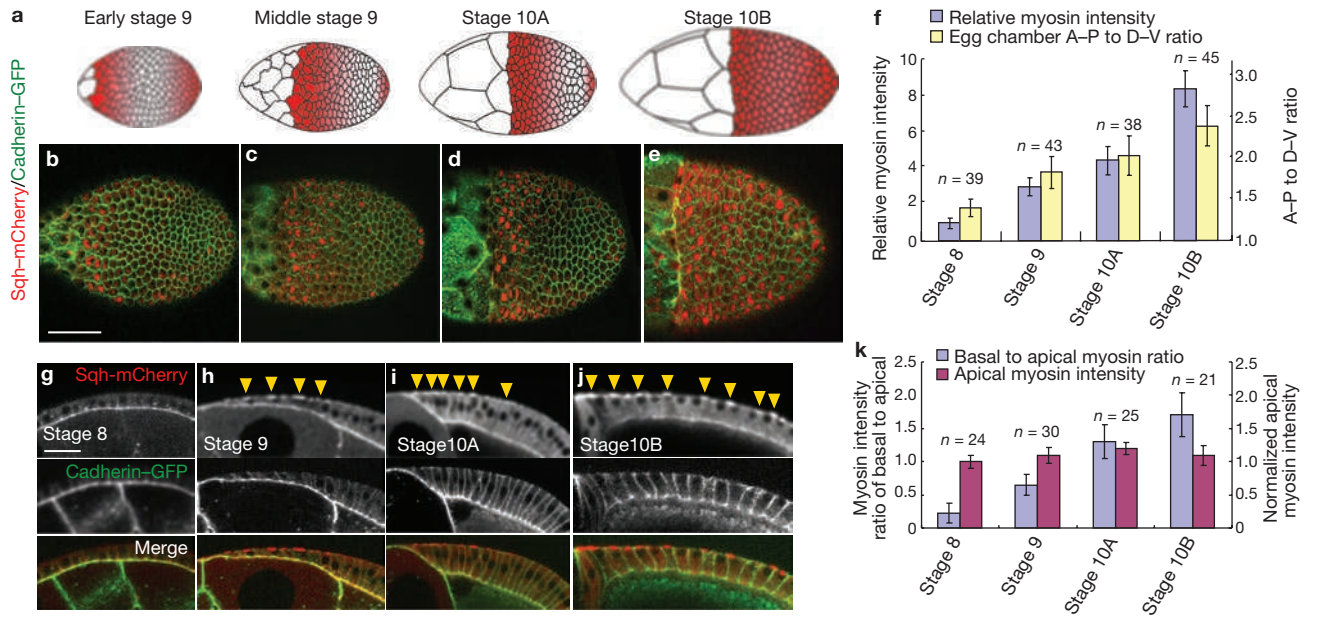

Figure 4 Global change in basal myosin during egg chamber development. (**a**) Schematic drawings of egg chambers at the indicated developmental stages. Red shading illustrates the overall distribution of cells with periodic myosin accumulation. Anterior is to the left. (**b**–**e**) Live egg chambers expressing Sqh–mCherry and cadherin–GFP at early stage 9 (**b**), middle stage 9 (**c**), stage 10A (**d**) and stage 10B (**e**). Scale bar, 50 μm. (**f**) Basal myosin intensity relative to stage 8 and ratio of A–P to D–V egg chamber length at different stages. A–P or D–V length was defined as the maximum distance between two points of the tissue in the corresponding direction. (**g**–**j**) Side views of follicle cells from egg chambers of the indicated stages, showing the increase in basal myosin and comparatively constant apical myosin through development. Arrows indicate sites of basal myosin accumulation. Scale bar, 15 μm. (**k**) Apical myosin intensity normalized to stage 8, and the ratio of basal myosin intensity (in cells that exhibit basal myosin accumulation) to apical myosin in the indicated number (*n*) of cells from stages 8–10.

that a contracting actomyosin network generates active forces to restrict the width of the tissue, resulting in its elongation (Fig. 5g, i).

Effect of the Rho–ROCK pathway and cell adhesion on myosin assembly and tissue shape

To explore the molecular mechanisms regulating actomyosin contractility further, we tested the function of the small GTPase Rho, which regulates the formation of actin stress fibres and myosin contractility in other contexts[24], and its effector kinase ROCK (Supplementary Information, Movie 8). Clones of follicle cells expressing a dominant-negative form of Rho (RhoN19) failed to accumulate basal myosin, whereas neighbouring wild-type follicle cells did so normally (Fig. 6a, b, i). In contrast, cells expressing the constitutively active form RhoV14 maintained a constant high level of basal myosin (Fig. 6c, i) and failed to relax (Supplementary Information, Movie 8). We then investigated ROCK, which can activate myosin[24]. Cells expressing a ROCK RNA-mediated interference (RNAi) construct, like RhoN19-expressing cells, lost basal myosin (Fig. 6d, i) and stopped oscillating (Supplementary Information, Movie 8), as did cells in egg chambers treated with the ROCK inhibitor Y-27632 (ref. 25) (Supplementary Information, Fig. S3a, k, p). Global knockdown of ROCK in all follicle cells also made the egg chamber rounder than the control (Fig. 6j–m, r), without any overall change in epithelium architecture. Significantly, apical actomyosin was little affected by ROCK RNAi, supporting the notion that the basal contraction was responsible for the effect (Fig. 6i; Supplementary Information, Figs S4h and S5h, q).

The parallel basal actin filaments are essential for egg chamber elongation[13,26–29]. Alignment of these filaments and ECM fibres has been suggested to function as a 'molecular corset', restricting the increase in tissue volume to the ends of the egg chamber[10–12,27]. Blocking integrin-mediated adhesion of follicle cells to the ECM also disrupts egg chamber elongation[13,26]. We therefore investigated the relationship between basal contractions and the cell–ECM interaction. To test the effect of cell–matrix adhesion on the oscillations in basal follicle cells, we knocked down the expression of talin, which is essential for integrin-mediated adhesion[30]. Basal myosin intensity decreased by 50% in mutant follicle cells (Fig. 6e, i; Supplementary Information, Movie 9). Paxillin is also an important linker between integrin and F-actin, overexpression of which enhances cell–matrix adhesion[31,32], and we found that paxillin overexpression increased myosin intensity by 60% (Fig. 6f, i; Supplementary Information, Movie 9). Neither talin knockdown nor paxillin overexpression had any detectable effect on the apical actomyosin network (Fig. 6i; Supplementary Information, Figs S4j, l and S5j, l, q). Global talin knockdown caused a round egg phenotype (Fig. 6n, o, r), whereas paxillin overexpression elongated egg chambers (Fig. 6p, q, r); this is consistent with their respective changes in basal myosin intensity.

We then tested whether cell–cell adhesion had any effect on the basal oscillation. Although cadherin is markedly enriched in subapical adherens junctions between follicle cells, it is also present all over basolateral cell surfaces, including at the level of the basal actin filament bundles (Supplementary Information, Fig. S6k). Cells expressing E-cadherin RNAi lost the basal actin and myosin filaments (Fig. 6g, i; Supplementary Information, Figs S4m, n and S5m, n, q), whereas overexpression of E-cadherin caused no detectable effect (Fig. 5h, i). Thus the basal actin network requires cadherin-mediated cell–cell adhesion, in a similar manner to basal actin stress fibres in cultured endothelial cells[33].

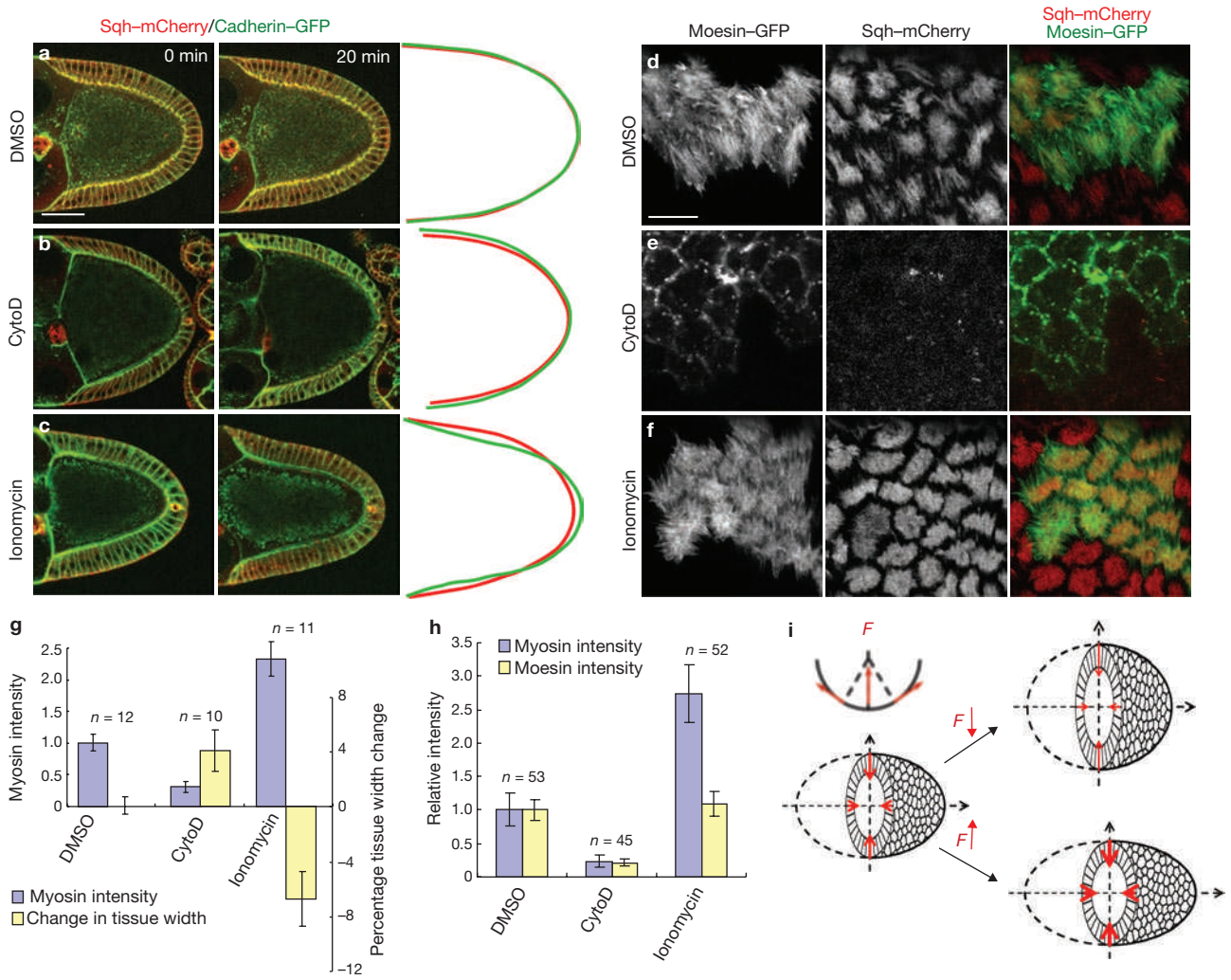

Figure 5 Basal actomyosin contractions control tissue shape. (**a**–**c**) Confocal micrographs of egg chambers treated with vehicle (DMSO, **a**), cytochalasin D (CytoD, **b**) or ionomycin (**c**) at 0 min (the beginning of imaging) and 20 min. Tissue contours at the two time points are shown at the right as red (0 min) and green (20 min) outlines. Scale bar, 50 μm. Control experiments and combination effects are shown in Supplementary Information, Fig. S3h–q. (**d**–**f**) Live images of basal F-actin (labelled with moesin–GFP) and myosin (Sqh–mCherry) after treatment for 30 min with DMSO (**d**), CytoD (**e**) or ionomycin (**f**). Scale bar, 10 μm. The more than 80% decrease in basal moesin–GFP signal after treatment with CytoD (**e**) suggests that most GFP intensity represents F-actin. Ionomycin showed little or no effect on basal F-actin (**f**). Treatment with ROCK and calcium inhibitors decreased myosin intensity to near background but had little effect on actin (Supplementary Information, Fig. S3a–c), suggesting that the formation of basal actin and myosin contractile fibres is regulated independently. (**g**) Average basal myosin intensity and percentage change in egg chamber width during the 20-min imaging time after treatment with the indicated drugs; *n* is the number of samples analysed. (**h**) Quantification of basal moesin–GFP and myosin intensity after treatment with the indicated drugs; *n* is the number of cells analysed. All error bars indicate s.d. (**i**) An illustration of the proposed mechanism by which follicle cell relaxation or contraction leads to tissue rounding or elongation. As a result of curvature of the egg chamber, contractile force (*F*) generated at the basal side is exerted in part towards the centre. The red arrowheads indicate different magnitudes of contractile forces.

Cell autonomy and regulation of the amplitude and period of the basal oscillations

In the mosaic analysis we noticed that wild-type cells surrounded by either constitutively relaxing (expressing RhoN19 or ROCK RNAi) or contracting (expressing RhoV14) neighbouring cells still oscillated with normal amplitude and period, demonstrating that the basal oscillation is a cell-autonomous behaviour (Fig. 7a–d; Supplementary Information, Movie 8).

To investigate the factors controlling the amplitude or period of the basal oscillations, we changed the extracellular or cytosolic calcium concentration or applied different concentrations of the ROCK inhibitor Y-27632. Buffering of extracellular calcium with EGTA did not alter the myosin oscillations (Supplementary Information, Fig. S3h, i, p). However, buffering intracellular calcium with BAPTA decreased the myosin intensity, and increasing intracellular calcium levels with ionomycin had the opposite effect (Supplementary Information, Fig. S3i, n–p). Although the basal myosin intensity changed markedly, as long as there was still a detectable oscillation the period remained largely unchanged (Fig. 7e, f). This was consistent with the observation that in wild-type tissue, follicle cells at different positions or developmental stages have different amplitudes of myosin oscillation but similar periods (Fig. 7g). This result implies that although ROCK activity and the presence of proper cytosolic calcium levels are necessary for maximal myosin accumulation, they may not be essential components of the oscillator. In contrast, altering integrin-mediated cell–ECM adhesion changed the oscillation period together with the myosin amplitude. Cells

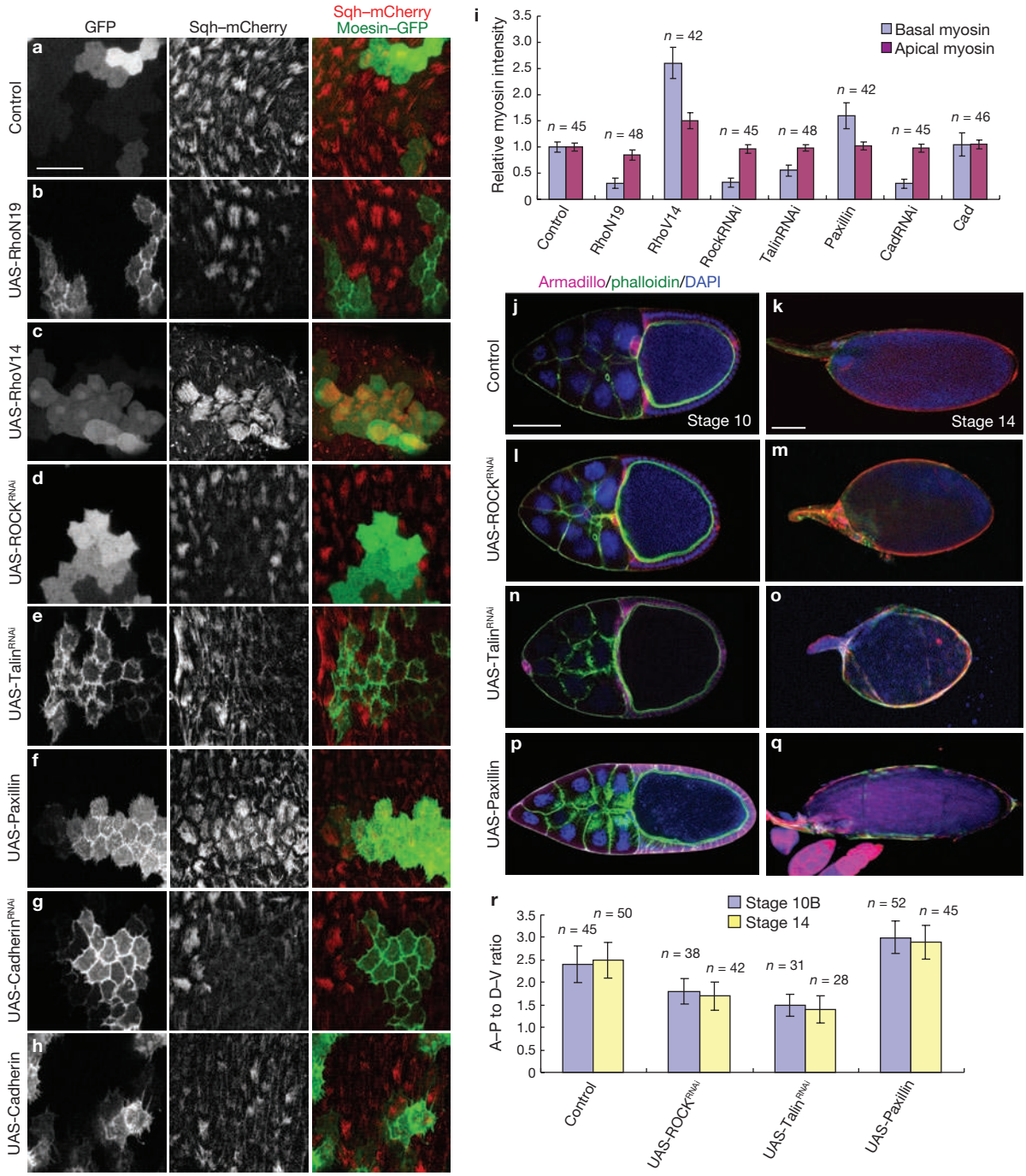

Figure 6 Rho, ROCK and cell adhesion regulate basal myosin accumulation and organ shape. (**a**–**h**) Basal view of follicle cell clones expressing the indicated transgenes, marked by co-expression of either nlsGFP (nuclear localization signal fused to GFP) or mCD8GFP (murine lymphocyte receptor CD8 transmembrane domain fused to GFP). Scale bar, 20 μm. (**i**) Quantification of relative basal and apical myosin intensities in the indicated number (*n*) of GFP-positive cells compared with wild-type cells in the same sample. Corresponding apical myosin and apical and basal actin images are shown in Supplementary Information, Figs S4 and S5. Verification of RNAi knockdown and overexpression is shown in Supplementary Information, Fig. S6. (**j**–**q**) Morphology of stage-10B (**j**, **l**, **n**, **p**) and stage-14 (**k**, **m**, **o**, **q**) egg chambers expressing the indicated transgene in all follicle cells. Egg chambers expressing *hs*Gal4 served as controls. DAPI, 4′,6-diamidino-2-phenylindole. Scale bar, 50 μm. (**r**) Quantification of the A–P to D–V length ratio in stage-10B and stage-14 egg chambers with the indicated genetic backgrounds; *n* is the number of samples analysed. In contrast, no significant difference was observed at late stage 8 (Supplementary Information, Fig. S7). All error bars are s.d.

expressing talin RNAi had a shorter period (4 min on average), whereas cells overexpressing paxillin had a longer period (9.3 min on average) (Fig. 7h–j). These results suggest that increasing cell–matrix adhesion slows the period of the oscillator, possibly by providing more mechanical resistance.

DISCUSSION

We have described a novel behaviour of epithelial cells, specifically a patterned, oscillating, basal epithelial myosin assembly and contraction. Previous work suggested that the polarized basal F-actin bundles and

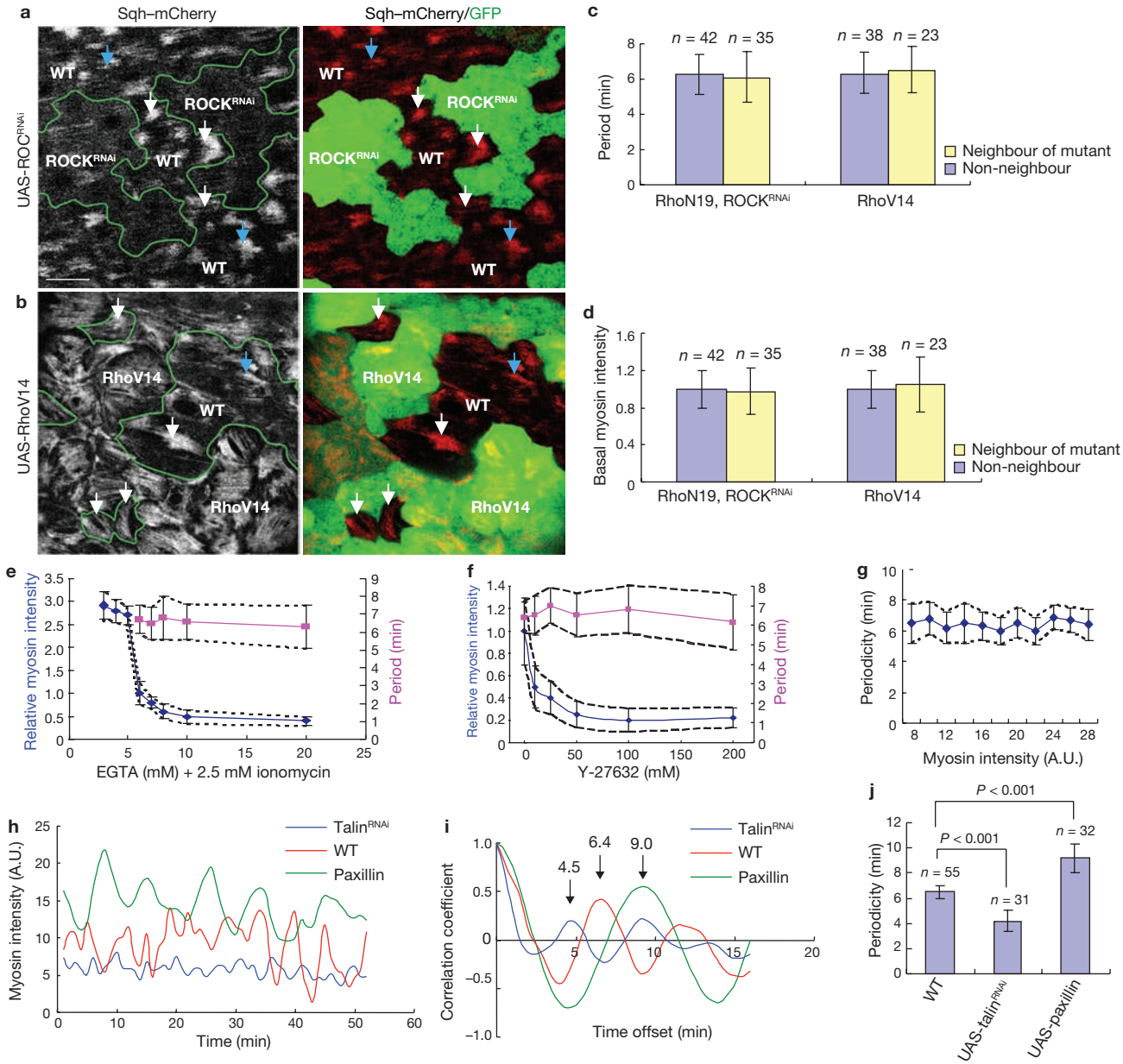

Figure 7 Cell autonomy of myosin oscillation and pathways affecting its magnitude and period. (**a**, **b**) Confocal micrographs of follicle cell clones in living egg chambers expressing Sqh–mCherry. (**a**) Wild-type (WT, GFP-negative) cells adjacent to cells expressing ROCK RNAi (GFP-positive) are indicated by white arrows. Wild-type cells without any contact with ROCK RNAi-expressing cells are indicated by blue arrows. Scale bar, 10 μm. (**b**) Wild-type (WT, GFP-negative) cells adjacent to cells expressing RhoV14 (GFP-positive) are indicated by white arrows. A wild-type cell without any contact with RhoV14 -expressing cells is identified by a blue arrow. (**c**, **d**). Quantification of myosin intensity and oscillation period in wild-type cells adjacent to mutant cells showed no significant difference from those in wild-type cells not adjacent to mutant cells; *n* is the number of individual cells analysed. (**e**) Basal myosin intensity and oscillation period after addition of different concentrations of EGTA together with 2.5 μM ionomycin. A total of 48 individual cells were analysed, covering about 150 periods. (**f**) Basal myosin intensity and oscillation period after treatment with various concentrations of the ROCK inhibitor Y-27632. A total of 37 cells were analysed, covering about 110 periods. (**g**) Plot of oscillation period against basal myosin intensity in wild-type egg chambers. Samples were collected from 65 individual cells, covering more than 200 periods. (**h**) Dynamics of basal myosin intensity in a representative individual cell expressing UAS-talin RNAi, UAS-paxillin or no UAS transgene (WT). (**i**) Autocorrelation with different time offsets from data in **h**. The first peak for each line provides the period for the corresponding genotype. (**j**) Quantification of the effect on period; *n* is the number of cells from three independent clones analysed. All error bars indicate s.d.

their integrin-mediated attachment to the surrounding basement membrane function as a corset, implying a static structure that constrains growth of the egg chamber to the poles, thus promoting tissue elongation[10–12]. Here we show that the 'corset' is dynamic and is composed of the periodic assembly and disassembly of myosin on the actin filaments, providing an explanation for the source of the necessary force. Contraction transiently diminishes the basal surface area of the affected follicle cells; however, this is not permanent, and we propose that it is not the most significant consequence of the contraction. Instead, the force generated by the contraction propagates inward towards the germline

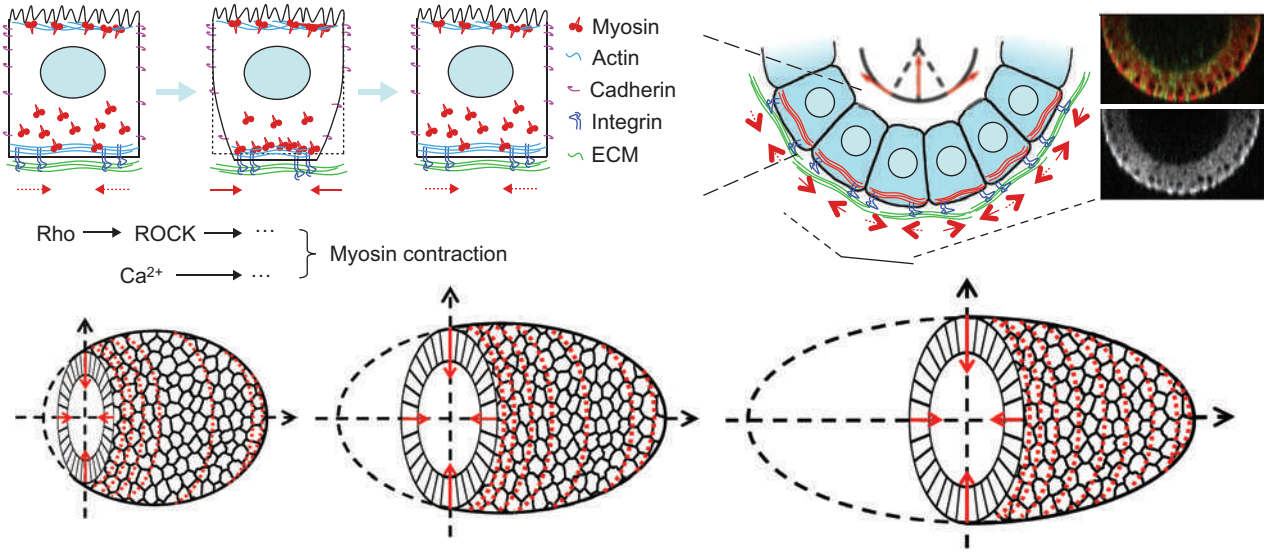

Figure 8 Model of tissue elongation controlled by basal actomyosin contraction. A schematic representation is shown of the distribution of molecules controlling oscillating basal contraction in an individual follicle cell and the organization of contractile forces into a super cellular band within the epithelium. Forces are indicated by red arrows. Local contraction force generated by basal myosin (red) transmitted through adhesions (blue) to the basal lamina (cyan) constrains tissue growth to the poles. Micrographs show a corresponding section through the middle of a stage-10 egg chamber labelled with cadherin–GFP and Sqh–mCherry. The Sqh–mCherry channel on its own is shown in black and white.

and opposes the outward force caused by growth. Because the oscillations occur near the centre of the egg chamber, expansion is directed preferentially to the poles. The oscillations are not synchronized; different cells therefore contract at different times and over the course of more than 10 h generate a sustained inward force.

These observations raise several questions. For example, what is the biochemical mechanism of the oscillation? Myosin activity oscillates in many (but not all) biological contexts. For example, cardiomyocytes beat in cell culture. However, this oscillation does not show or require cycles of myosin assembly and disassembly; it is driven by ion fluxes and is much more rapid (150 beats min^{-1}) than the oscillations described here (average period 6–7 min). Myosin has intrinsic biochemical properties that could in principle lead to oscillating assembly and disassembly on this timescale[34]. Three properties, in combination, could contribute to oscillation: the intrinsic mechanochemical cycle of actin binding, power stroke, and dissociation from actin; thick filament assembly–disassembly dynamics; and actin filament anchoring. Myosin II assembly into thick filaments is tension-dependent[35,36]. That is, as myosin begins to assemble on actin filaments, it exerts force on them, generating tension if the filaments are anchored. If the resistance is great enough, myosin will stall in the isometric state rather than completing its power stroke and disassociating from the actin filament[34]. As a consequence, more and more myosin filaments assemble over time. In addition, the binding of myosin to actin becomes highly cooperative in response to tension. Thus more myosin molecules bind and they dissociate more slowly when there is tension. For myosin to sense and respond to tension, the actin filaments to which it is bound must be prevented from sliding. During cytokinesis in *Dictyostelium*, the critical actin anchor is the actin crosslinker cortexillin[37]. However, in principle, anchoring to the plasma membrane could also serve this purpose. We found in *Drosophila* follicle cells that myosin assembles on F-actin stress fibres that are attached through integrin, talin and paxillin to ECM fibres. This probably serves the critical function of anchoring actin filaments so that tension is generated when myosin binds. So, what causes disassembly and leads to oscillations? When enough myosin molecules assemble for the force per myosin head to become sufficiently small, the myosins can complete their power strokes and disassociate from actin, resulting in disassembly of myosin thick filaments. Stochastically, new myosins bind, exert force, experience tension and recruit more myosin, and the cycle repeats.

Increasing the load against which myosin works would be expected to increase the number of myosin molecules that assemble as well as the length of time until the force per unit molecule has decreased to the point of disassembly. In other words, increasing the mechanical resistance should increase both the amplitude and the period of myosin oscillations. Our results suggest that the actin–integrin–ECM interaction provides the load and explains why decreasing follicle-cell–ECM adhesion decreases both the period and amplitude of the oscillation and why enhancing cell–ECM interaction increases both. This explanation is also consistent with the observation that the assembly–disassembly cycle that occurs during ventral furrow formation in the embryo has a shorter period (about 1 min). In this case the cycle occurs on the apical side of the cell, where there is no basement membrane to provide mechanical resistance. Although there may be additional components to the oscillation mechanism, these elements would in principle be sufficient to cause oscillating assembly and disassembly of myosin.

In contrast to most previously studied morphogenetic processes, in which cells change the shape of a tissue by altering their own geometry, follicle cells undergoing this basal contraction do not change their own shape permanently but instead generate forces that constrain the shape of the underlying tissue (Fig. 8). Another morphogenetic process that involves two cell layers is branching morphogenesis of the developing mammary gland[38]. In this case, outer myoepithelial cells may help sculpt the underlying glandular epithelium, constraining growth towards the terminal end buds. It will be of interest to determine whether basal actomyosin activity in the epithelial layer also contributes to the morphogenesis of this or other organs and tissues in which expansion is constrained.

The observation that this oscillation shares some characteristics with other actomyosin oscillations, such as that occurring during apical constriction, and yet differs in numerous respects suggests that an intrinsic oscillator is subject to tissue specific regulation. This allows the oscillations to occur in some cells and at some stages of development but not others, near the apical cell surface in some cells or the basal side in others, and connected to a ratchet in some cells but not others. In addition, the period can be regulated in a cell-type-specific manner by adjusting the resistance against which the motor pulls. In each cell type in which it has been described, the observation of oscillations came as a surprise, because intuitively a static contractile force might seem to suffice. Whether or not oscillation is essential remains to be clarified. In any case, a complete understanding of the temporal and spatial patterning, subcellular localization and tuning of the oscillations will be necessary to realize the goal of reconstituting normal organ shapes and tissue architectures *in vitro*. □

METHODS

Methods and any associated references are available in the online version of the paper at http://www.nature.com/naturecellbiology/

Note: Supplementary Information is available on the Nature Cell Biology website.

ACKNOWLEDGEMENTS

We thank Doug Robinson for invaluable discussions, critical reading of the manuscript and help with writing the discussion of the myosin oscillation mechanism. Nick Brown and Eric Wieschaus generously donated reagents. This work was supported by grants to D.J.M. from the National Institute of General Medical Sciences including R01 GM46425, GM73164 and the Cell Migration Consortium. Bloomington *Drosophila* Stock Center and Vienna *Drosophila* RNAi Center resources contributed to this work. FlyBase provided important information used in this work. Clones provided by the Berkeley *Drosophila* Genome Project and distributed by *Drosophila* Genetic Resource Center were used.

AUTHOR CONTRIBUTIONS

L.H. and X.W. performed the image acquisition and mutant analysis. L.H. processed and analysed images. H.L.T. conducted inhibitor treatments and calcium-related experiments. D.J.M. prepared the manuscript. All authors participated in the interpretation of the data and the production of the final manuscript.

COMPETING FINANCIAL INTERESTS

The authors declare no competing financial interests.

Published online at http://www.nature.com/naturecellbiology
Reprints and permissions information is available online at http://npg.nature.com/reprintsandpermissions/

1. Lecuit, T. & Lenne, P. F. Cell surface mechanics and the control of cell shape, tissue patterns and morphogenesis. *Nat. Rev. Mol. Cell Biol.* **8,** 633–644 (2007).
2. Mammoto, T. & Ingber, D. E. Mechanical control of tissue and organ development. *Development* **137,** 1407–1420 (2010).
3. Martin, A. C., Kaschube, M. & Wieschaus, E. F. Pulsed contractions of an actin–myosin network drive apical constriction. *Nature* **457,** 495–499 (2009).
4. Solon, J., Kaya-Copur, A., Colombelli, J. & Brunner, D. Pulsed forces timed by a ratchet-like mechanism drive directed tissue movement during dorsal closure. *Cell* **137,** 1331–1342 (2009).
5. Bertet, C., Sulak, L. & Lecuit, T. Myosin-dependent junction remodelling controls planar cell intercalation and axis elongation. *Nature* **429,** 667–671 (2004).
6. Horne-Badovinac, S. & Bilder, D. Mass transit: epithelial morphogenesis in the *Drosophila* egg chamber. *Dev. Dyn.* **232,** 559–574 (2005).
7. Wu, X., Tanwar, P. S. & Raftery, L. A. *Drosophila* follicle cells: morphogenesis in an eggshell. *Semin. Cell Dev. Biol.* **19,** 271–282 (2008).
8. Wang, Y. & Riechmann, V. The role of the actomyosin cytoskeleton in coordination of tissue growth during *Drosophila* oogenesis. *Curr. Biol.* **17,** 1349–1355 (2007).
9. Kolahi, K. S. *et al.* Quantitative analysis of epithelial morphogenesis in *Drosophila* oogenesis: new insights based on morphometric analysis and mechanical modeling. *Dev. Biol.* **331,** 129–139 (2009).
10. Gutzeit, H. O. The microfilament pattern in the somatic follicle cells of mid-vitellogenic ovarian follicles of *Drosophila*. *Eur. J. Cell Biol.* **53,** 349–356 (1990).
11. Gutzeit, H. O., Eberhardt, W. & Gratwohl, E. Laminin and basement membrane-associated microfilaments in wild type and mutant *Drosophila* ovarian follicles. *J. Cell Sci.* **100,** 781–788 (1991).
12. Gutzeit, H. O. Organization and *in vitro* activity of microfilament bundles associated with the basement membrane of *Drosophila* follicles. *Acta Histochem. Suppl.* **41,** 201–210 (1991).
13. Bateman, J., Reddy, R. S., Saito, H. & Van Vactor, D. The receptor tyrosine phosphatase Dlar and integrins organize actin filaments in the *Drosophila* follicular epithelium. *Curr. Biol.* **11,** 1317–1327 (2001).
14. Prasad, M., Jang, A. C., Starz-Gaiano, M., Melani, M. & Montell, D. J. A protocol for culturing *Drosophila* melanogaster stage 9 egg chambers for live imaging. *Nat. Protocols* **2,** 2467–2473 (2007).
15. Prasad, M. & Montell, D. J. Cellular and molecular mechanisms of border cell migration analyzed using time-lapse live-cell imaging. *Dev. Cell* **12,** 997–1005 (2007).
16. Oda, H. & Tsukita, S. Real-time imaging of cell–cell adherens junctions reveals that *Drosophila* mesoderm invagination begins with two phases of apical constriction of cells. *J. Cell Sci.* **114,** 493–501 (2001).
17. Martin, A. C. Pulsation and stabilization: contractile forces that underlie morphogenesis. *Dev. Biol.* **341,** 114–125 (2010).
18. Martin, A. C., Gelbart, M., Fernandez-Gonzalez, R., Kaschube, M. & Wieschaus, E. F. Integration of contractile forces during tissue invagination. *J. Cell Biol.* **188,** 735–749 (2010).
19. David, D. J., Tishkina, A. & Harris, T. J. The PAR complex regulates pulsed actomyosin contractions during amnioserosa apical constriction in *Drosophila*. *Development* **137,** 1645–1655 (2010).
20. Blanchard, G. B., Murugesu, S., Adams, R. J., Martinez-Arias, A. & Gorfinkiel, N. Cytoskeletal dynamics and supracellular organisation of cell shape fluctuations during dorsal closure. *Development* **137,** 2743–2752 (2010).
21. Edwards, K. A., Demsky, M., Montague, R. A., Weymouth, N. & Kiehart, D. P. GFP–moesin illuminates actin cytoskeleton dynamics in living tissue and demonstrates cell shape changes during morphogenesis in *Drosophila*. *Dev. Biol.* **191,** 103–117 (1997).
22. Uehata, M. *et al.* Calcium sensitization of smooth muscle mediated by a Rho-associated protein kinase in hypertension. *Nature* **389,** 990–994 (1997).
23. Hilgers, R. H. & Webb, R. C. Molecular aspects of arterial smooth muscle contraction: focus on Rho. *Exp. Biol. Med.* **230,** 829–835 (2005).
24. Pellegrin, S. & Mellor, H. Actin stress fibres. *J. Cell Sci.* **120,** 3491–3499 (2007).
25. Narumiya, S., Ishizaki, T. & Uehata, M. Use and properties of ROCK-specific inhibitor Y-27632. *Methods Enzymol.* **325,** 273–284 (2000).
26. Frydman, H. M. & Spradling, A. C. The receptor-like tyrosine phosphatase lar is required for epithelial planar polarity and for axis determination within *Drosophila* ovarian follicles. *Development* **128,** 3209–3220 (2001).
27. Conder, R., Yu, H., Zahedi, B. & Harden, N. The serine/threonine kinase dPak is required for polarized assembly of F-actin bundles and apical-basal polarity in the *Drosophila* follicular epithelium. *Dev. Biol.* **305,** 470–482 (2007).
28. Viktorinova, I., Konig, T., Schlichting, K. & Dahmann, C. The cadherin Fat2 is required for planar cell polarity in the *Drosophila* ovary. *Development* **136,** 4123–4132 (2009).
29. Mirouse, V., Christoforou, C. P., Fritsch, C., St Johnston, D. & Ray, R. P. Dystroglycan and perlecan provide a basal cue required for epithelial polarity during energetic stress. *Dev. Cell* **16,** 83–92 (2009).
30. Brown, N. H. *et al.* Talin is essential for integrin function in *Drosophila*. *Dev. Cell* **3,** 569–579 (2002).
31. Conway, W. C. *et al.* Paxillin modulates squamous cancer cell adhesion and is important in pressure-augmented adhesion. *J. Cell. Biochem.* **98,** 1507–1516 (2006).
32. Schaller, M. D. Paxillin: a focal adhesion-associated adaptor protein. *Oncogene* **20,** 6459–6472 (2001).
33. Millan, J. *et al.* Adherens junctions connect stress fibres between adjacent endothelial cells. *BMC Biol.* **8,** 11 (2010).
34. Kee, Y. S. & Robinson, D. N. Motor proteins: myosin mechanosensors. *Curr. Biol.* **18,** R860–R862 (2008).
35. Kovacs, M., Thirumurugan, K., Knight, P. J. & Sellers, J. R. Load-dependent mechanism of nonmuscle myosin 2. *Proc. Natl Acad. Sci. USA* **104,** 9994–9999 (2007).
36. Fernandez-Gonzalez, R., Simoes, S. de M., Röper, J. C., Eaton, S. & Zallen, J. A. Myosin II dynamics are regulated by tension in intercalating cells. *Dev. Cell* **17,** 736–743 (2009).
37. Ren, Y. *et al.* Mechanosensing through cooperative interactions between myosin II and the actin crosslinker cortexillin I. *Curr. Biol.* **19,** 1421–1428 (2009).
38. Ewald, A. J., Brenot, A., Duong, M., Chan, B. S. & Werb, Z. Collective epithelial migration and cell rearrangements drive mammary branching morphogenesis. *Dev. Cell* **14,** 570–581 (2008).

METHODS

***Drosophila* stocks and genetics.** The following fly stocks were used: Ubi::DE-cadherin–GFP and Sqh::Sqh–mCherry (from Eric F. Wieschaus), UAS-moesin–GFP, UAS-RhoN19 and UAS-RhoV14 (from Bloomington *Drosophila* Stock Center), UAS-DE-cadherin^{RNAi}, UAS-ROCK^{RNAi} and UAS-talin^{RNAi} (from Vienna *Drosophila* RNAi Center[39]), and UAS-GFP–paxillin. *hs*Gal4/CyO, MKRS/TM6B flies were used to express UAS lines in all follicle cells. Clones were generated using FLP-OUT technique by crossing UAS transgenic flies with either P[*hsp*70-flp]; Sqh::Sqh–mCherry; UAS-mcd8GFP, *Ay*Gal4 or P[hsp70-flp]; UAS-nlsGFP, *Ay*Gal4; Sqh::Sqh–mCherry. For fixed sample, a FLP-OUT fly without Sqh::Sqh–mCherry was used. All stocks and crosses were maintained at room temperature. *hs*FLPase was induced for 1 h at 37 °C, and flies were then kept at either 29 °C or 31 °C for 2 days before dissection. *hs*Gal4 flies were incubated three times at 37 °C for 1 h each and flies were kept at 25 °C for 1–2 days before dissection.

DNA constructs and transgenic fly generation. Full-length paxillin complementary DNA was obtained from the *Drosophila* Genomics Resource Center and amplified by following primers: 5′-GGGGACAAGTTTGTACAAAAAAGCAGGCTTCAACATGGACGATTTGGATGCTCTAT-3′ (5 end) and 5′-GGGGACCACTTTGTACAAGAAAGCTGGGTGTCATCCGAATATCTTGTCGAAGCAG-3′ (3 end). The PCR product was first cloned into pDONR 221 vector (Invitrogen) using BP clonase II (Invitrogen). The insertion was then recombined into pUASt gateway vector with N-fusion of GFP (from DGRC) by LR clonase II (Invitrogen). UAS-GFP–paxillin flies were generated by Bestgene Inc. using w^{1118} flies. Flies with UAS-GFP–paxillin were crossed with *hs*Gal4; Sqh::Sqh–mCherry flies to test expression pattern and level. Expressed GFP–paxillin was enriched at the focal adhesion site as reported previously[40] (Supplementary Information, Fig. S6j).

Time-lapse image acquisition. *Drosophila* egg chambers were dissected and mounted in live imaging medium (Invitrogen Schneider's insect medium with 20% FBS and 0.1 mg ml^{-1} insulin) as described previously[14,15]. Egg chambers were slightly compressed to overcome the endogenous curvature. More glass spacers were used when capturing *z*-stack images of egg chambers without compression (Fig. 1a, b; Supplementary Information, Movie 1). The basal oscillation pattern, intensity and period were similar in both conditions. Fixed samples showed a similar pattern, suggesting that the myosin pattern was not an artefact of the culture condition (Supplementary Information, Fig. S1c–j). Time-lapse imaging was performed with a Zeiss 710 NLO-Meta confocal microscope with a 40×, numerical aperture 1.1 water-immersion lens, with a 488-nm argon laser and a 543-nm green HeNe laser. Imaging at 10-s intervals was tested at first. Because the average oscillation period is 6.3 min, we used a 60-s interval to prolong the imaging time for most of experiments unless specified otherwise.

The basal focal plane, which is about 1 μm beneath the basal surface, was selected during live imaging to maximize the basal myosin intensity. When imaging the apical side, the focal plane was selected on the basis of the clearest cadherin–GFP signal. The same microscope setup was used when comparing intensity between different samples.

Image processing and data analysis. For all images the background (intensity of area without sample) was subtracted. All displaced figures were processed with a Gaussian smoothing filter with a radius of one pixel to reduce noise. Three-dimensional reconstructions of egg chambers were generated by maximum projection (Supplementary Information, Movie 1) or transparent projection (to highlight the surface; Fig. 1a, c) from *z*-stacks with 1-μm intervals using Zeiss ZEN software (http://www.zeiss.de/zen).

Time-lapse cadherin–GFP images were processed with Image J as follows: images were first filtered with a Gaussian blur filter with radius of 25 pixels; the resulting images were subtracted from original images as local background, and the images were then segmented with a watershed algorithm plug-in[41]. The segmented images were corrected manually on the basis of the original images.

The processed images were analysed with MATLAB (MathWorks) to track individual cells and automatically calculate the cell area, A–P length and D–V length. A–P and D–V length were calculated by averaging the edge distance in each direction. The Sqh–mCherry channel was processed in MATLAB first to correct for photobleaching. Subsequently the intensity of an individual cell was calculated as the average value of all pixels within the cell area. A general cytosolic myosin signal contributed to the final results and represents about 20% of the average myosin signal.

For myosin (red) and moesin (green) dual-colour imaging, the intensity of moesin–GFP or Sqh–mCherry was calculated from manually outlined cell areas, as was the myosin intensity in mutant clones because cadherin–GFP was not present to mark cell boundaries.

The distribution of oscillation periods was generated by measuring the intervals between each pair of adjacent peaks. The myosin signals were used because they were less noisy than the surface area. We applied autocorrelation to calculate the period of a time series with different time offsets. The location of the first peak greater than zero indicates the shortest period contained in the series. This method averages out irregularities in the sequence and gives a similar average period (Fig. 2h). We found that autocorrelation was more robust and provided better results in analysing irregular signals with a small amplitude, such as the myosin intensity in talin knockdown cells (Fig. 7h–j). Therefore the analysis of period in all experiments other than Fig. 2b was calculated by autocorrelation.

The time series data were smoothed with a Gaussian filter, with σ equal to three data points. The basal contraction rate was calculated as the inverse value of the first derivative of basal area. The rate of change of intensity was the first derivative of intensity. Data for correlation were collected with a 30-s interval to catch subtle phase differences. Cross-correlation efficiency was calculated with time shift from –9 to +9 min. The heat map was constructed by correlations from different individual cells with the correlation coefficient coded in rainbow colouring. The averaged correlation coefficient was generated by averaging smoothed correlation data from tested cells.

Myosin intensity was analysed by using egg chambers from early to middle stage 10 because of the widespread and reliable basal myosin pattern. Anterior columnar follicle cells were used in quantification because of their consistent behaviour. The change of the one measured variable was defined as two standard deviations above and two standard deviations below the mean. An unpaired two-sided *t*-test was performed with Excel (Microsoft).

Small-molecule and other treatments. Egg chambers were dissected in live imaging medium with chemicals at the indicated final concentrations, and then mounted for imaging. The following chemicals and final concentrations were used: F-actin destabilizer cytochalasin D (20 μg ml^{-1}; Sigma), the calcium ionophore ionomycin (2.5 μM; Invitrogen), the microtubule destabilizer colchicine (50 μg ml^{-1}; Sigma), the ROCK inhibitor Y-27632 (200 μM; Sigma) and the cytosolic calcium chelator bis-(*o*-aminophenoxy)ethane-*N*,*N*,*N*′,*N*′-tetra-acetic acid acetoxymethyl ester (BAPTA-AM, 50 μM; Invitrogen). For treatment with BAPTA, the non-ionic detergent Pluronic F-127 (Invitrogen) was applied to the medium at a final concentration of 0.02% to facilitate dispersion of the AM ester in aqueous medium. Sample was incubated with BAPTA-AM and Pluronic F-127 for 1 h and then washed and recovered in BAPTA-AM-free medium for another 15 min before microscopy. Quantification of change in egg chamber shape after drug treatment used the images taken at the start (0 min) and the end (20 min) of live imaging (not including about 10 min used in mounting and microscope preparation after addition of the drug). An image of the middle (sagittal) plane of the egg chamber was used. Tissue width was calculated by dividing the area of the posterior half of the egg chamber (the oocyte and its associated columnar follicle cells) by its A–P length.

DMSO or ethanol (5% for colchicine) was used as control. The effect of ionomycin can be blocked by adding 5 mM EGTA or 200 μM Y-27632 after incubation for 1 min with ionomycin, whereas the addition of 10 mM EGTA had no immediate effect. Prolonged incubation with EGTA caused endocytosis of cadherin and loss of basal myosin. Ionomycin (2.5 μM) immediately reversed the effect of BAPTA. The effect of treatment with Y-27632 can also be reversed by 2.5 μM ionomycin together with 5 mM $CaCl_2$.

Dosage-dependent effects of ROCK inhibition on basal myosin were tested by applying different concentrations of Y-27632 (0–200 μM) for 1 h before live imaging. To control the Ca^{2+} concentration, component-defined *Drosophila* Ringer's buffer (with 2 mM Ca^{2+}) was used. Because of nutrient limitations, egg chambers can survive for only about 2 h in this medium, in contrast with about 6–8 h in live imaging medium. However, the basal contraction seemed normal. Samples were first treated with 2.5 μM ionomycin for 1 min, followed by the addition of different concentrations of EGTA; samples were then immediately imaged for 30–50 min.

DOI: 10.1038/ncb2124

Immunohistochemistry. *Drosophila* ovaries were dissected in Schneider's medium and fixed with 4% formaldehyde for 20 min. Antibody staining was performed as decribed previously[42]. Anti-talin antibody (1:100 dilution) was a gift from N. H. Brown[30], and anti-DE-cadherin antibody (rat anti-dCAD2, 1:10) and anti-Armadillo antibody (mouse N27A1, 1:50 dilution) were from the Developmental Studies Hybridoma Bank. Secondary antibodies conjugated with Alex-568 and Alexa-647 (Molecular Probes) were used in 1:300 dilutions. Alexa-568-conjugated phalloidin (1:300 dilution; Invitrogen) was used for F-actin staining. Samples were imaged on a Zeiss LSM 510-Meta confocal microscope.

RT–PCR analysis. *hs*Gal4;UAS-RNAi was used to knock down the specific targets in all ovary follicle cells (Supplementary Information, Fig. S6a–i). Flies were heat-shocked at 37 °C for 1 hour, six times over 2 days. After recovery for 1 day, total RNA was extracted from whole flies with an RNeasy Mini kit (Qiagen 74104), and was quantified by measuring A_{260}. For RT–PCR, 1 μg of RNA was reverse-transcribed with Superscript RNase H-RT (Invitrogen) in the presence of 100 ng of oligo(dT) (Invitrogen). PCR for different targets was performed in a thermal cycler in the following cycle: 95 °C for 30 s, 55 °C for 30 s and 72 °C for 60 s; for 20–24 cycles of E-cadherin, ROCK or Talin. The actin primer reaction required 16 cycles. The following primers were used: cadherin, 5′-GGATACGCTCCTAAGGTCAA-3′ (forward1), 5′-CCGACTCCTTGTCAATCTTG-3′ (reverse1), 5′-GACGAGTGTCTGATTGAGAAG-3′ (forward2) and 5′-ATCTTGGTGTTGTTGCAGGC-3′ (reverse2); ROCK, 5′-GAGAAACTGTGACCAAGCAG-3′ (forward1), 5′-GAGAACCACCTCCATTGTGT-3′ (reverse1), 5′-CAAGGACGAAGAGATCACCA-3′ (forward2) and 5′-CAATCGATCTCCATGACCAT-3′ (reverse2); Talin, 5′-CATACAGTTCCAGCCCAACA-3′ (forward1), 5′-TCTGCCTCATCTATTCCCTG-3′ (reverse1), 5′-CAAACACCTTCACTCTGGAC-3′ (forward2) and 5′-TGCGAACTTCCTTAGTCGTG-3′ (reverse2); actin, 5′-GGAGAAGCTGTGCTATGTTG-3′ (forward) and 5′-TGATGGAGTTGTAGGTGGTC-3′ (reverse).

39. Dietzl, G. *et al.* A genome-wide transgenic RNAi library for conditional gene inactivation in *Drosophila*. *Nature* **448,** 151–166 (2007).
40. Delon, I. & Brown, N. H. The integrin adhesion complex changes its composition and function during morphogenesis of an epithelium. *J. Cell Sci.* **122,** 4363–4374 (2009).
41. Vincent, L. & Soille, P. Watersheds in digital spaces—an efficient algorithm based on immersion simulations. *IEEE Trans. Pattern Anal. Machine Intell.* **13,** 583–598 (1991).
42. McDonald, J. A. & Montell, D. J. Analysis of cell migration using *Drosophila* as a model system. *Methods Mol. Biol.* **294,** 175–202 (2005).

nature cell biology

DOI: 10.1038/ncb2124

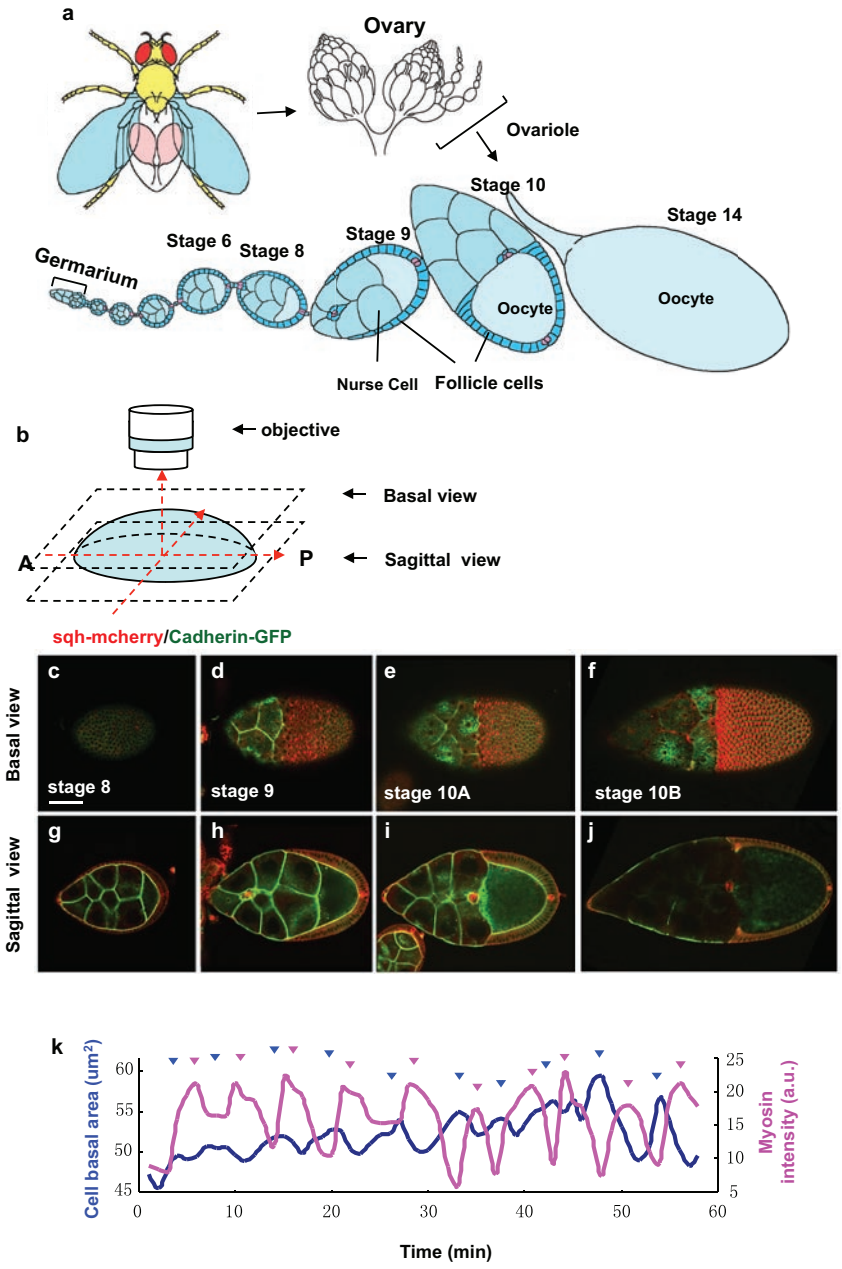

FigureS1 Imaging egg chamber at different developmental stages and basal surface and myosin activity. **a.** Schematic drawings of a female fruit fly, a pair of ovaries, the ovarioles that make up the ovary and the egg chambers that make up the ovariole. Egg chambers form in the germarium from somatic (follicle cells) and germline cells (oocyte and nurse cells). Early stage egg chambers are round. Elongation occurs between stages 6 and 14. From stage 6 to early stage 9, the A-P:D-V ratio increases from 1.0 to 1.5. However, from stage 9 to stage 10B, this ratio increases to 2.5 while the volume of the egg chamber increases almost ~8 fold. **b.** A diagram of imaging setup indicating the basal and sagittal focal planes used throughout this study. **c-j.** Confocal microscope images of fixed egg chambers of the indicated stages expressing Cadherin-GFP (green) and Sqh-mcherry (red). Basal views **(c-f)** and corresponding sagittal views **(g-j)**. Scale bar is 50 μm. **k.** Graph plotting the change of basal cell area and myosin intensity from a single cell over time. Each peak is indicated by an arrowhead.

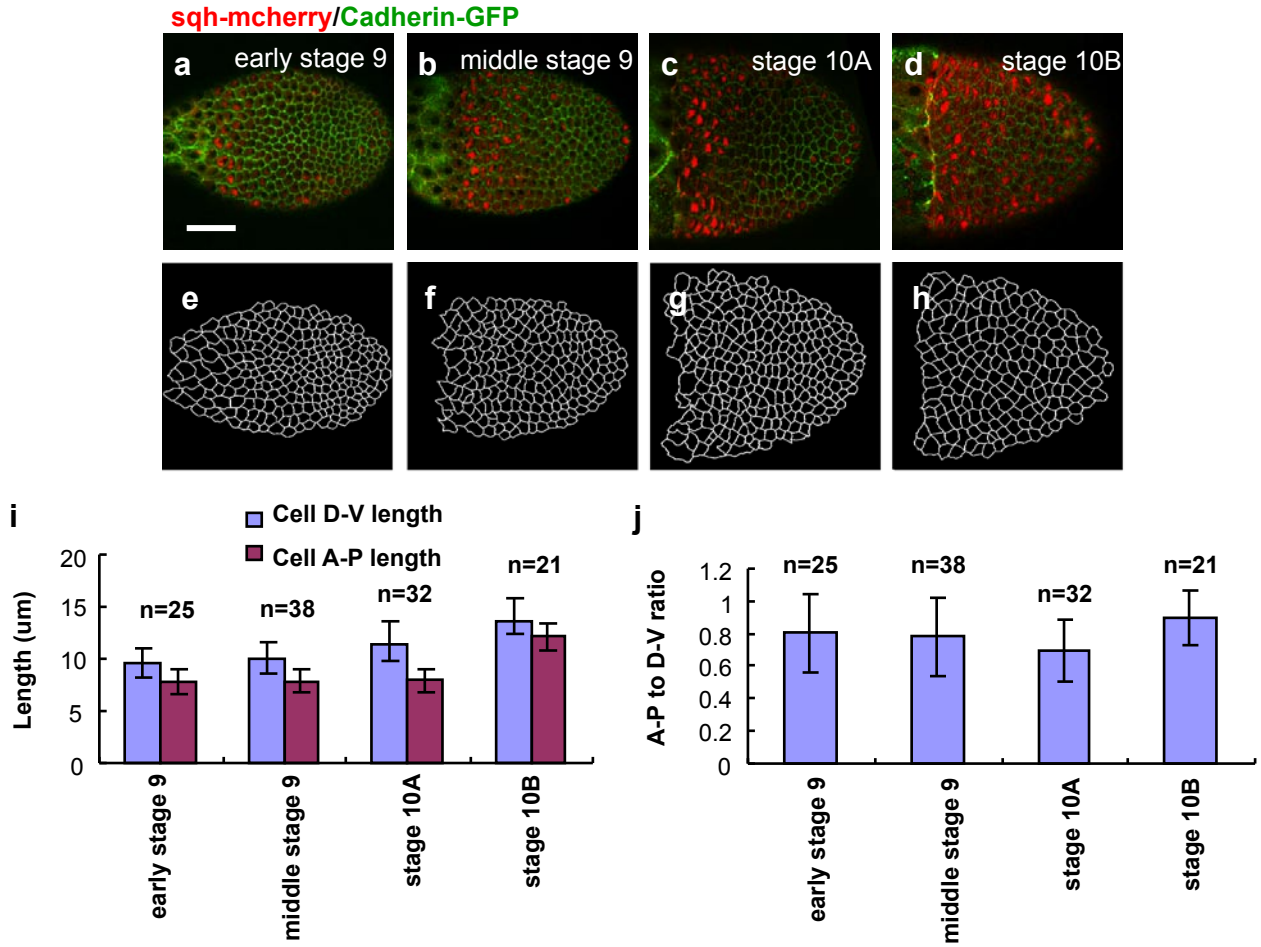

Figure S2 Characterization of basal myosin accumulation and changes in cell basal area and shape. **a-h.** Representative live egg chambers expressing both cadherin-GFP and sqh-mcherry at early stage 9 **(a)**, middle stage 9 **(b)**, stage 10A **(c)** and stage 10B **(d)**. Edges of follicle cells at corresponding stage **(e-h)** were calculated using a watershed algorithm (see methods). Scale bar is 40μm. **i,j.** Change of cell D-V length and A-P length (**i**) and their ratio from early stage9 to stage 10B (**j**). n is the number of individual cell analyzed. Error bars indicate ±s.d..

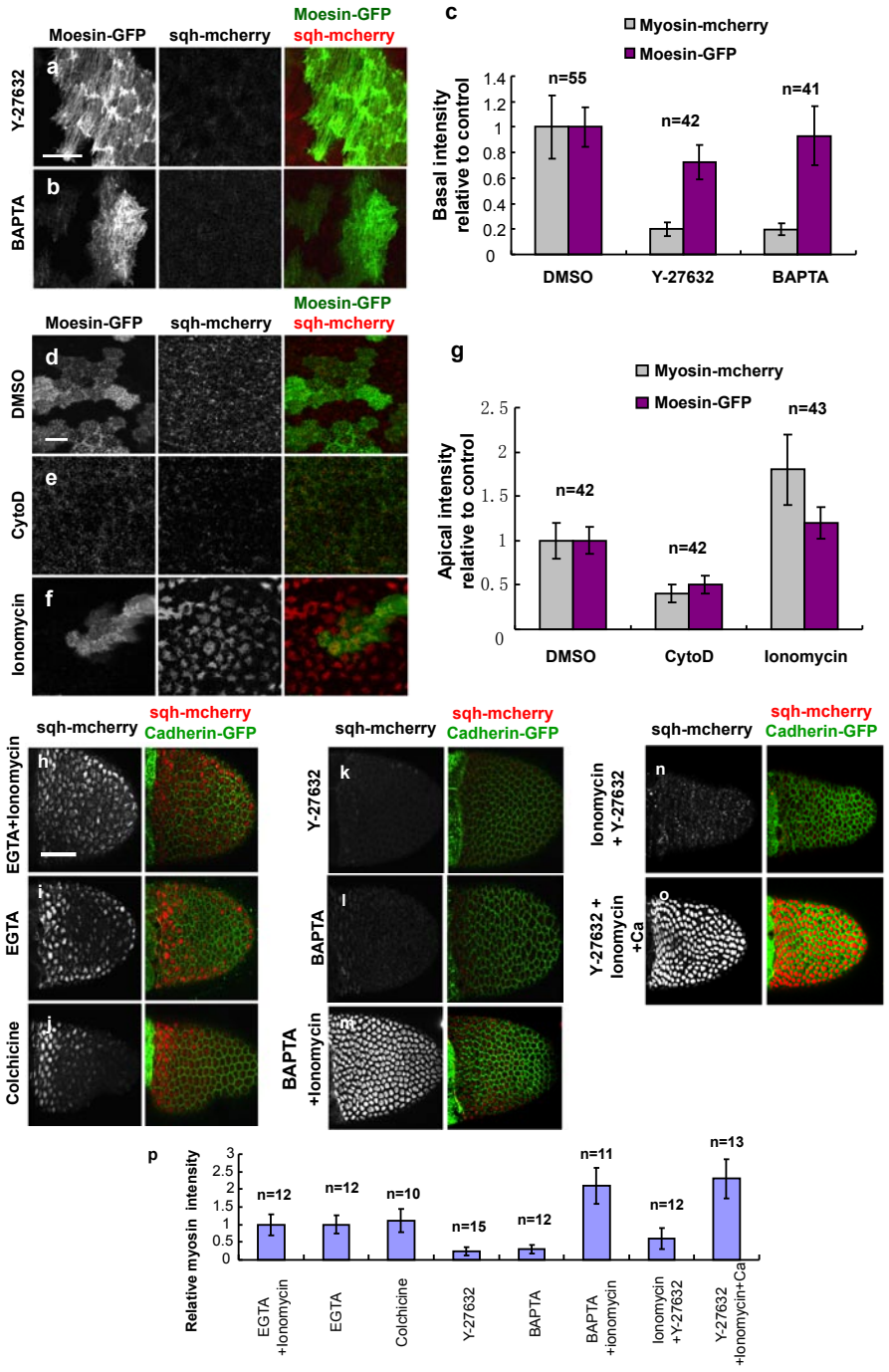

Figure S3 Pharmacological manipulation of basal F-actin and myosin. **a,b.** A Moesin-GFP expressing follicle cell clone was imaged after treatment with the ROCK inhibitor Y-27632 (**a**) or the cytosolic calcium chelator BAPTA (**b**). Scale bar is 10μm. No significant change of apical moesin-GFP was observed and apical myosin was moderately reduced for both treatments (data not shown). **c.** Quantification of basal moesin and myosin intensity under indicated treatment conditions for the indicated numbers (n) of cells. **d-f**. Live images of apical F-actin (labeled with Moesin-GFP) and myosin (Sqh-mcherry) after 30 min treatment of DMSO, CytoD or ionomycin. Scale bar is 10μm. **g.** Quantification of apical Moesin-GFP and myosin intensity after treatments. n is the number of cells analyzed. **h-q.** Confocal micrographs of living egg chambers expressing Cadherin-GFP (green) and Sqh-mcherry (red) following treatments with the indicated agents. The effect of ionomycin was neutralized by addition of 5mM EGTA **(h)**, while EGTA alone had no effect **(i)**. **j.** Destabilizing microtubules with colchicine had no substantial effect on basal myosin. **k.** The ROCK inhibitor Y-27632 strongly inhibited the basal myosin, as did the calcium chelator BAPTA **(l)**. The effect of BAPTA can be reversed by ionomycin **(m)**. Addition of Y-27632 to the ionomycin pretreated egg chambers, or addition of ionomycin together with extra Ca^{2+} into Y-27632 pretreated egg chamber reversed the effects on myosin **(n, o)**. Scale bar is 50μm. **p.** Quantification of basal actin intensity in egg chambers with indicated treatments. All intensities were normalized on wild-type (WT) egg chamber. n is the number of individual egg chambers analyzed. Error bars indicate ±s.d..

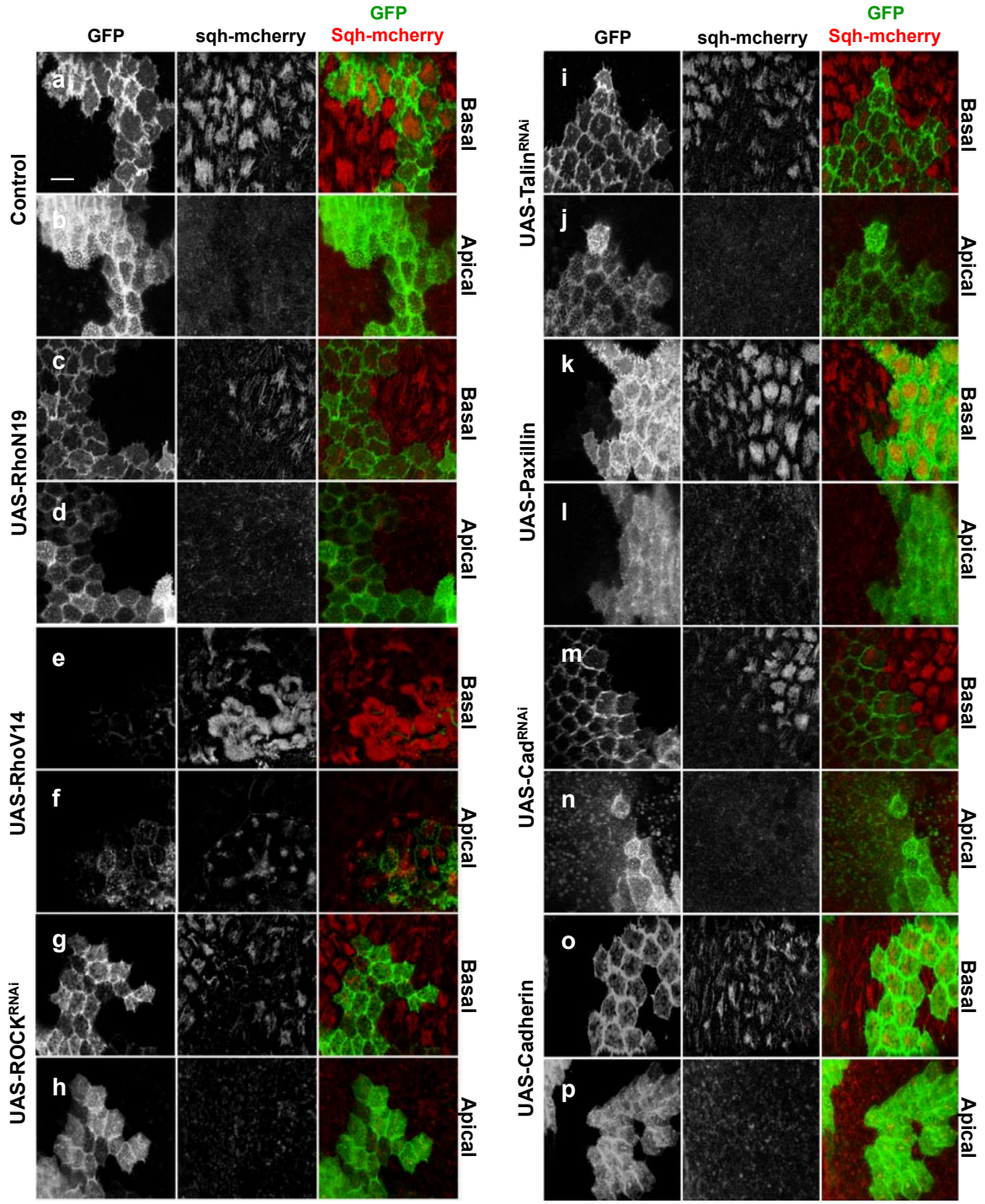

Figure S4 Effects of Rho, ROCK, and cell adhesions on apical and basal myosin. **a-p.** Confocal micrographs of follicle cell clones (GFP+) expressing the indicated transgenes and myosin was visualized by sqh-mcherry (red) in live egg chambers. For each genotype, up-panel was the basal image while bottom-panel was the apical image. Scale bar is 10μm.

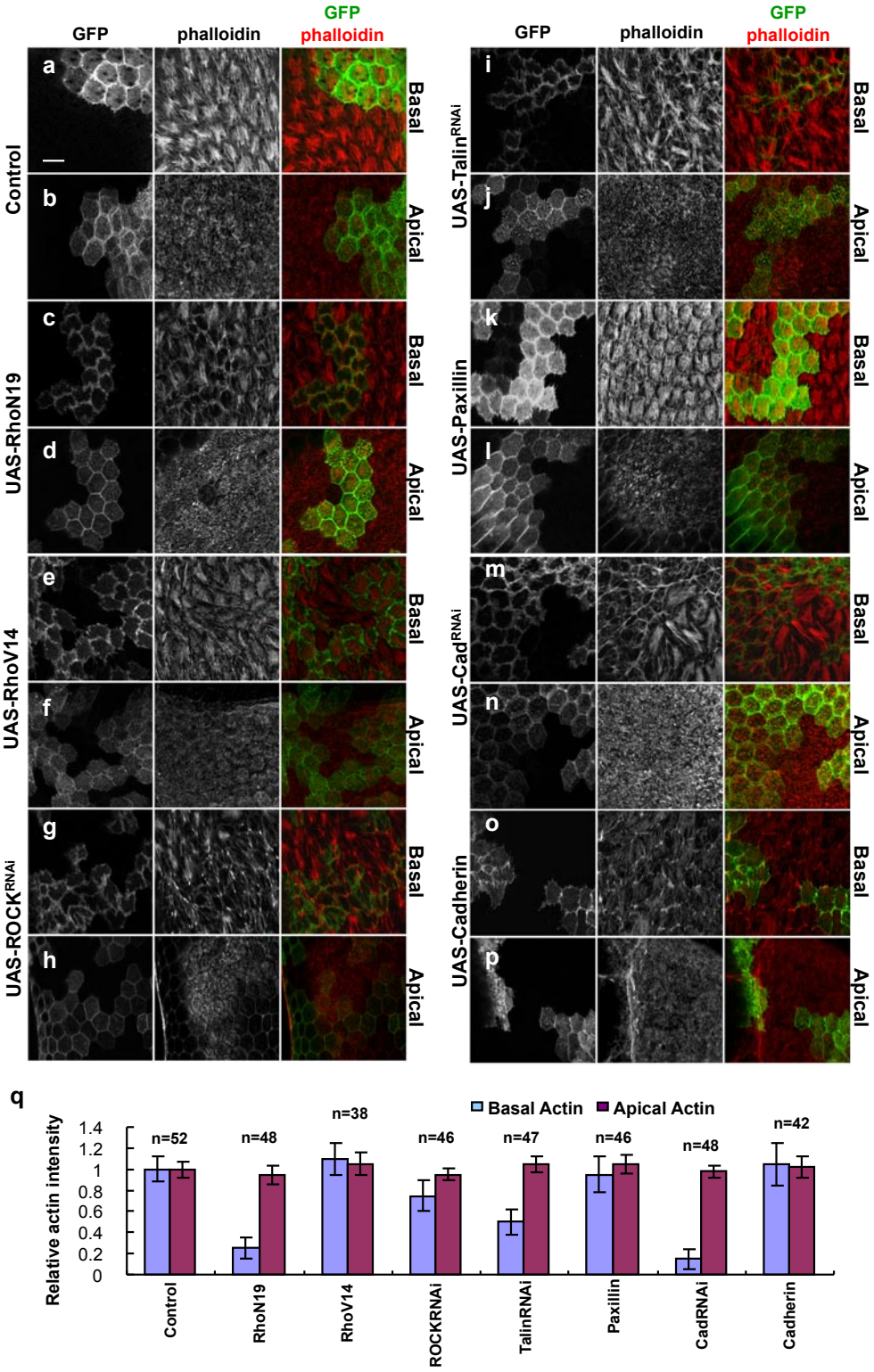

Figure S5 Effects of Rho, ROCK, and cell adhesions on apical and basal F-actin. **a-p.** Confocal micrographs of follicle cell clones (GFP+) expressing the indicated transgenes and F-actin was stained by phalloidin (red) in fixed egg chambers. For each genotype, up-panel was the basal image while bottom-panel was the apical image. Scale bar is 10μm. **q.** Quantification of apical and basal actin intensity in cells expressing the indicated transgenes. All intensities were normalized to WT cells. n is the number of individual cell analyzed. Error bars indicate ±s.d..

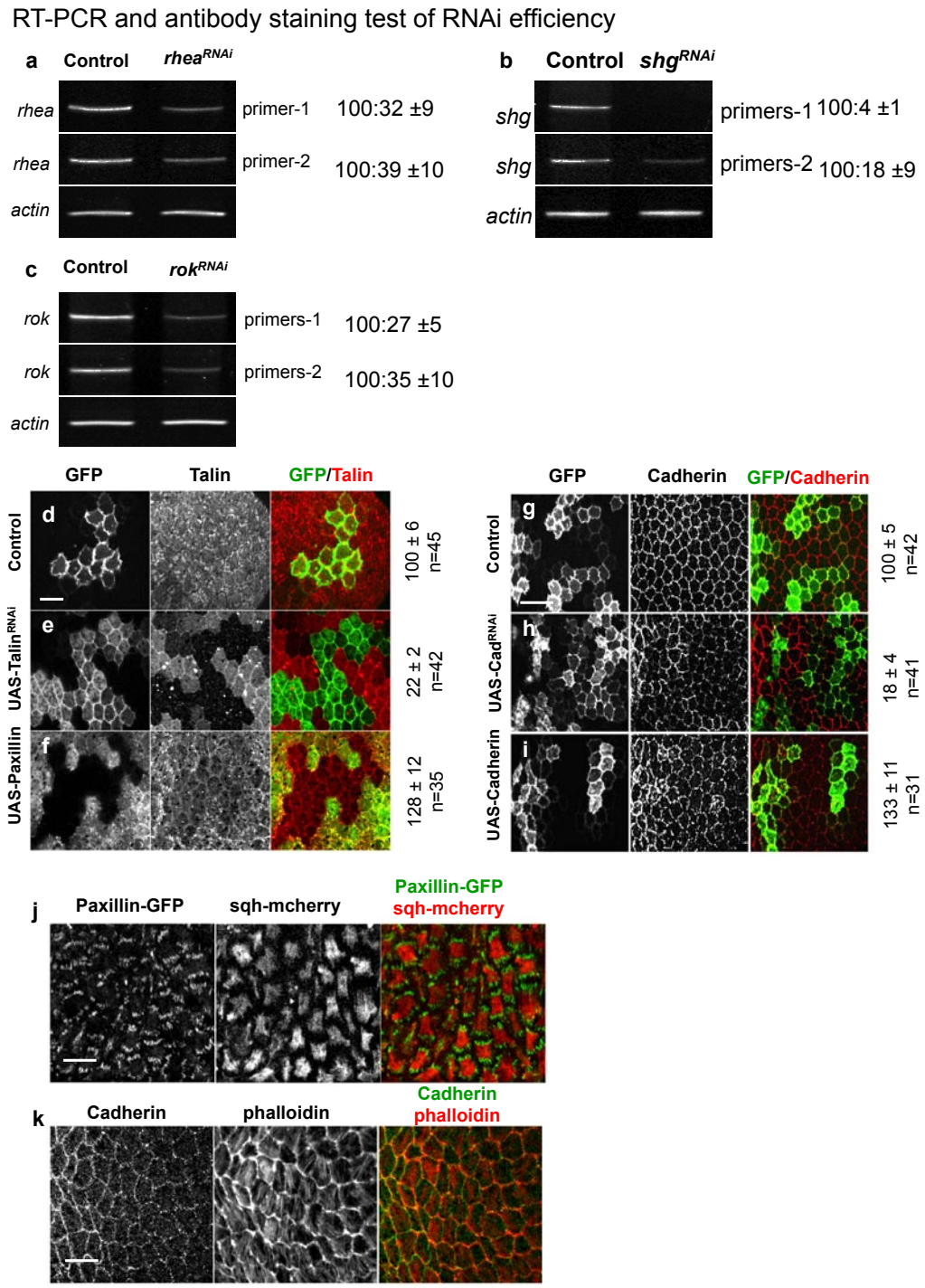

Figure S6 Efficacy of RNAi, Paxillin localization, and presence of basal cadherin. **a-c.** RT-PCR experiments showed efficient knock-down of mRNA level of target genes. **a.** Talin is encoded by the *rhea* gene. Two different primer sets revealed a 60-70% reduction in talin mRNA. **b.** E-cadherin is encoded by the *shg* gene. Two different primer sets revealed an 80-95% reduction in shg mRNA. **c.** Rho kinase is encoded by the *rok* gene. Two different primer sets revealed a 65-70% reduction in *rok* mRNA. Numbers on the right of each panel indicate average percentage ±s.d.. **d-f,** Confocal micrographs of follicle cell clones expressing GFP alone (Control) or GFP together with Talin RNAi or paxillin overexpression, stained with an anti-Talin antibody (red). Moderate increased Talin staining was observed in paxillin overexpressing cells, consistent with enhanced cell-ECM adhesion. **g-i,** Confocal micrographs of follicle cell clones expressing GFP alone (Control) or GFP with Cadherin RNAi or over-expressing Cadherin, stained with an anti-Cadherin antibody (red). Scale bar is 20μm. Quantification of staining intensity was indicated with WT intensity set to 100. n is the number of cells analyzed. **j.** Expressed paxillin was detected by its GFP tag (green) and myosin was labeled by sqh-mcherry. This localization was consistent with previous reported focal adhesion sites in follicle cells. Scale bar is 10μm. **k.** Cadherin (green) was detected by antibody, F-actin (red) was stained by phalloidin. Cadherin also exists at the basal focal plane together with basal F-actin. Scale bar is 10μm.

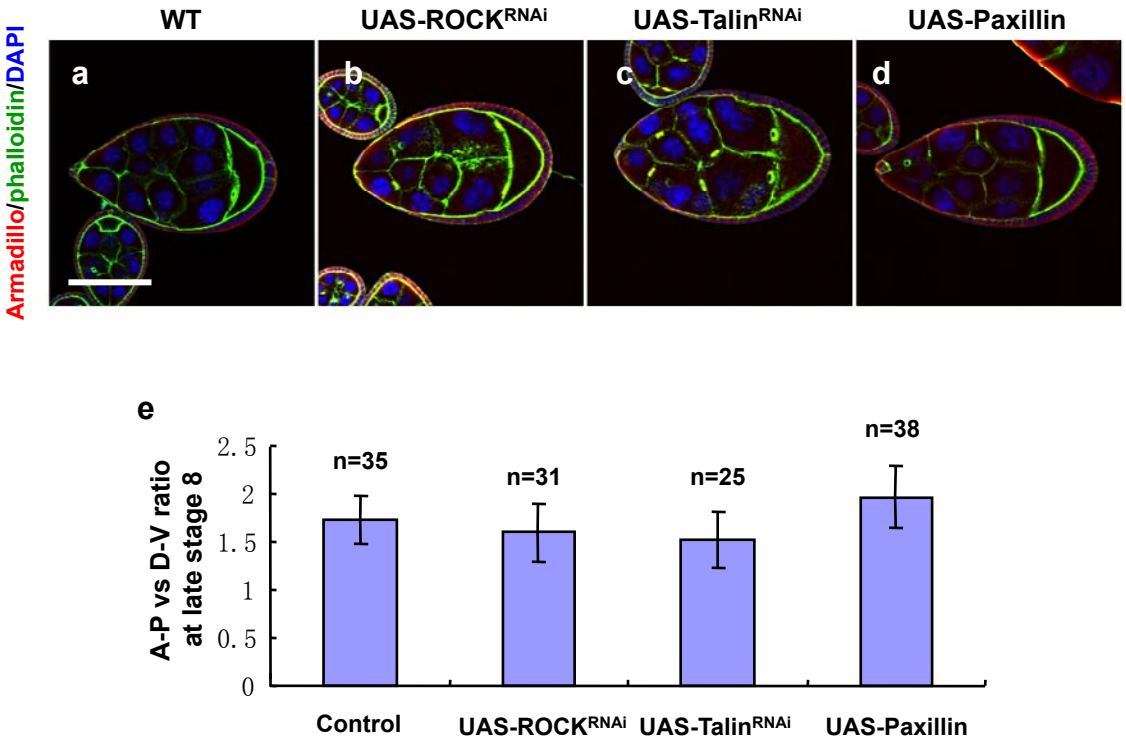

Figure S7 Egg chamber elongation before stage 9. **a-d.** Representative late stage 8 egg chambers expressing the indicated transgenes in all follicle cells using heat shock inducible Gal4. Scale bar is 50 μm. **e.** Quantification of egg chamber elongation at late stage 8 showed no significant effects, suggesting the differences at later stages were not caused by early defects. n is the number of the tissue analyzed. Error bars indicate ±s.d..

Supplementary movie legends

Movie S1 Monitoring cadherin and myosin in follicle cells in living stage 9 egg chambers. 3D maximum intensity projection from z-stacks of a living Drosophila egg chamber at late stage 9. Cells were labeled with Cadherin-GFP (green) together with Sqh-mcherry (red). Some cells show a patch of myosin fibers near the basal cell surface. In timelapse series these cells contract.

Movie S2 Periodic cell contractions near the basal surface**.** Timelapse series of confocal images of follicle cells expressing Cadherin-GFP (green) and Sqh-mcherry (red) in living egg chambers. Left, a field of cells labeled with cadherin-GFP (green) and sqh-mcherry (red). Focus is near the basal surface. Right, a Watershed algorithm was used to digitize the cadherin-GFP signal for quantitative measurements of dynamic changes in cell length and area.

Movie S3 Apical follicle cell surfaces are less dynamic and myosin does not accumulate periodically. Timelapse series of confocal images of follicle cells expressing Cadherin-GFP (green) and Sqh-mcherry (red) in living egg chambers. Left, a field of follicle cells labeled with cadherin-GFP (green) and Sqh-mcherry (red). Focus is near the apical surface. Right, digitized cadherin-GFP signal allows quantitative measurements of cell length and area.

Movie S4 Comparison of lateral and basal views**.** Timelapse series of confocal images of follicle cells expressing Cadherin-GFP (green in left panels) and Sqh-mcherry (red in left panels, white in right panels) in living egg chambers. Top panels show side views of the oscillations, demonstrating that myosin does not move in and out of the basal plane of focus as no accumulation is observed more apically. Bottom views show a basal plane of focus where myosin assembles and disassembles in basal fibrillar arrays.

Movie S5 Basal F-actin fibers do not disassemble**.** Timelapse series of confocal images of follicle cells in living egg chambers. UAS-Moesin-GFP (green in left panel) labels F-actin and was expressed in a clone of cells using the FLP-OUT technique. Sqh-mcherrry (red in left panel) was expressed ubiquitously. Changes in F-actin intensity were much smaller than changes in myosin intensity (see also Fig. 2c).

Movie S6 Global patterns of myosin accumulation and activity**.** Timelapse series of confocal images of follicle cells expressing Cadherin-GFP (green) and Sqh-mcherry (red) in living egg chambers to visualize global patterns of periodic basal myosin accumulation and contraction during development. Early stage 9 (ES9), mid stage 9 (MS9), stage 10A (S10A) and stage 10B (S10B). The contractions first appear early in stage 9 in the anterior 1/3 of the egg chamber. Then the contracting band shifts posteriorly to the middle of the tissue, grows stronger, and spreads to include most follicle cells contacting the oocyte. The sqhamous cells covering the nurse cells do not exhibit periodic myosin accumulation or cell contractions.

Movie S7 Effects of cytochalasin and ionomycin on myosin accumulation and tissue shape. Timelapse series of confocal images of living egg chambers expressing Cadherin-GFP (green) and Sqh-mcherry (red) treated with vehicle (DMSO), Cytochalasin D (CytoD), or ionomycin. Top panels show a basal view and reveal the effects of the drugs on myosin accumulation as well as cell and tissue contraction/relaxation. Bottom panels show a slice through the center of the egg chamber and show the overall effect on tissue expansion or elongation.

Movie S8 Effects of Rho and ROCK on myosin accumulation and dynamics**.** Timelapse series of confocal images of follicle cells in living egg chambers expressing Sqh- mcherry (red in top panels, white in bottom panels). GFP positive cells are clones of cells expressing either GFP only (control), GFP and dominant-negative Rho (UAS-RhoN19), GFP and constitutively active Rho (UAS-RhoV14), or GFP and an RNAi line for Rho kinase (UAS-ROCK^{RNAi}).

Movie S9 Effect of cell-matrix adhesion on myosin accumulation and dynamics. Timelapse series of confocal images of clones of GFP positive follicle cells expressing Sqh-mcherry (red in top panels, white in bottom panels) together with either GFP only (control), or GFP and Talin RNAi (UAS-Talin^{RNAi}) or GFP and UAS-GFP-Paxillin.

Movie S10 Effect of cell-cell adhesion on myosin accumulation and dynamics. Timelapse series of confocal images of clones of GFP positive follicle cells expressing Sqh-mcherry (red in top panels, white in bottom panels) together with either GFP only (control), GFP and Cadherin RNAi (UAS-Cadherin^{RNAi}), or GFP and UAS-Cadherin.